

RAN Slicing for Massive IoT and Bursty URLLC Service Multiplexing: Analysis and Optimization

Peng Yang, Xing Xi, Tony Q S Quek, *Fellow, IEEE*, Jingxuan Chen, Xianbin Cao, *Senior Member, IEEE*, Dapeng Wu, *Fellow, IEEE*

Abstract

Future wireless networks are envisioned to serve massive Internet of things (mIoT) via some radio access technologies, where the random access channel (RACH) procedure should be exploited for IoT devices to access the networks. However, modelling of the dynamic process of RACH of massive IoT devices is challenging. To address this challenge, we first revisit the frame and minislot structure of the radio access network (RAN). Then, we correlate the RACH request of an IoT device with its queue status and analyze the evolution of the queue status. Based on the analysis result, we derive the closed-form expression of the random access (RA) success probability of the device. Besides, considering the agreement on converging different services onto a shared infrastructure, we investigate the RAN slicing for mIoT and bursty ultra-reliable and low latency communications (URLLC) service multiplexing. Specifically, we formulate the RAN slicing problem as an optimization one to maximize the total RA success probabilities of all IoT devices and provide URLLC services for URLLC devices in an energy-efficient way. A slice resource optimization (SRO) algorithm exploiting relaxation and approximation with provable tightness and error bound is then proposed to mitigate the optimization problem.

Index Terms

Massive IoT, random access channel, bursty URLLC, RAN slicing

P. Yang and T. Q S Quek are with the Information Systems Technology and Design, Singapore University of Technology and Design, 487372 Singapore.

X. Xi, J. Chen, and X. Cao are with the School of Electronic and Information Engineering, Beihang University, Beijing 100083, China, and also with the Key Laboratory of Advanced Technology, Near Space Information System (Beihang University), Ministry of Industry and Information Technology of China, Beijing 100083, China.

D. Wu is with the Department of Electrical and Computer Engineering, University of Florida, Gainesville FL 32611 USA.

I. INTRODUCTION

With the explosive growth of the Internet of Things (IoT), massive IoT (mIoT) devices, the number of which is predicted to reach 20.8 billion by 2020, will access the wireless networks for implementing advanced applications. These applications include e-health, public safety, smart traffic, virtual navigation/management, and environment monitoring. To address the IoT market, the third-generation partnership project (3GPP) has identified mIoT as one of the three main use cases of 5G and has already initiated several task groups to standardize several solutions including extended coverage GSM (EC-GSM), LTE for machine-type communication (LTE-M), and narrowband IoT (NB-IoT) [1], [2]. For establishing massive connections among wireless networks and mIoT devices, the research on reliable and efficient access mechanisms should be prioritized. In accomplishing the massive connections, when an IoT device wants to transmit signals in the uplink, it randomly chooses a random access (RA) preamble from an RA preamble pool and transmits it through an RA channel (RACH). If more than one device tries to access a base station (BS) simultaneously, then interference occurs at the remote radio head (RRH).

A. Prior arts

During the past few years, a rich body of works [3]–[5] on RA mechanisms has been developed to mitigate interference and improve the RA success probability or reduce the access delay of an IoT device. For example, the work in [3] proposed to improve the RA success probability of an IoT device by exploiting a distributed queue mechanism and then proposed an access resource grouping mechanism to reduce the access delay caused by the queuing process of the distributed queue mechanism. The work in [4] proposed a novel scheme to increase RA success probability. First, this scheme increased the number of preambles at the first step of the RA procedure by utilizing a spatial group mechanism. Second, it improved resource utilization through non-orthogonally allocating uplink channel resources at the second step of the RA procedure. Besides, to reduce the access delay, a grant-free non-orthogonal RA system relying on the accurate user activity detection and channel estimation was proposed in [5].

Most of the studies [3]–[5], however, assumed that network resources were reserved for the IoT service and did not study the case of the coexistence of IoT service and many other services such as enhanced mobile broadband (eMBB) and ultra-reliable and low latency communications (URLLC). The research of the coexistence of IoT service and other services is essential as future networks are convinced to integrate various services with different latency, reliability, and

throughput requirements into a shared physical infrastructure rather than deploying individual network solution for each type of service [6]. What is more, owing to the shared characteristic of network resources, some conclusions obtained in the case of providing sole IoT service may become inapplicable if multiple types of services are required to be supported by the networks.

Network slicing is considered as a promising technique in future networks to converge various services onto a shared physical infrastructure via partitioning the infrastructure into multiple network slices, where a network slice is defined as an end-to-end virtual network running on the infrastructure, capable of providing a negotiated service quality [7]. Recently, many slicing frameworks have been developed to provide performance guarantees for IoT or massive machine-type communications (mMTC) service, eMBB service and URLLC service [8]–[11]. For example, instead of slicing the radio access network (RAN) via orthogonal resource allocation among various services, the work in [8], [9] studied the advantages of allowing for non-orthogonal RAN resources sharing in uplink communications from a set of mMTC, eMBB, and URLLC users to the same BS. The work in [10] developed a two-level scheduling process to allocate dynamically dedicated bandwidth to each slice based on workload demand and slices' quality of service (QoS) requirement such that flexible resource allocation could be implemented. Besides, in [11], we proposed to orchestrate network resources for a network slicing system to guarantee more reliable URLLC and energy-efficient eMBB service provisions.

B. Motivation and contributions

Unlike the work in [3]–[5], [8]–[11], this paper simultaneously analyzes the RA process for the mIoT service and studies the RAN slicing for the mIoT service included service multiplexing. This study is highly challenging because i) performance requirements of a massive number of IoT devices should be satisfied. Yet, the typical 5G cellular IoT, NB-IoT can admit only 50,000 devices per cell [12], and the 5G new radio (NR) technique can only connect a great number of devices by deploying costly ultra-dense heterogeneous networks; ii) RAN slicing operation (e.g., activating and releasing slices) has to be conducted in a timescale of minutes to hours to keep pace with the upper layer network slicing. In the process of slicing upper layer networks, some functions (e.g., radio resource control function) and protocols (e.g., RAN protocol stacks) should be activated and configured, which are time-consuming [7]. However, wireless channels generally change in a timescale of millisecond to seconds. The RAN slicing should tackle the issue of operating RAN slicing based on time-varying channels, called a two timescale issue

[13]; iii) compared with the resource allocation problem for the eMBB service, the resource allocation problem for the bursty URLLC service where URLLC packets arrive in burst may be more challenging due to the stringent high reliability and low latency requirement.

These challenges motivate us to investigate the RAN slicing for mIoT and bursty URLLC service provision to maximize the utility of mIoT slices and that of bursty URLLC slices. The main contributions of this paper can be summarized as the following: 1) We revisit the frame and minislot structure for mIoT transmissions to accommodate more RA requests from a massive number of IoT devices; 2) We adopt a queueing model to capture the IoT packet arrival, accumulation and departure processes and analyze the queue evolution process by employing probability and stochastic geometry theories. Based on the analysis result, we derive the closed-form expression of the RA success probability of a randomly chosen IoT device; 3) We define mIoT slice utility and bursty URLLC slice utility and formulate the RAN slicing for mIoT and bursty URLLC service multiplexing as a resource optimization problem. The objective of the optimization problem is to maximize the total mIoT and URLLC slice utilities, subject to limited physical resource constraints. The solution of this problem is difficult due to the existence of indeterministic objective function and thorny non-convex constraints and the requirement of tackling a two timescale issue as well; 4) To mitigate this thorny optimization problem, we propose a slice resource optimization (SRO) algorithm. In this algorithm, we first exploit a sample average approximate (SAA) technique and an alternating direction method of multipliers (ADMM) to tackle the indeterministic objective function and the two timescale issue. Then, a semidefinite relaxation (SDR) scheme joint with a Taylor expansion scheme are leveraged to approximate the non-convex problem as a convex one. The tightness of the SDR scheme and the error bound of the Taylor expansion are also analyzed.

It is noteworthy that the optimization method is exploited to investigate the service multiplexing of mIoT and URLLC in this paper. As the optimization method has a powerful generalization ability, this paper can be extended to the multiplexing of more types of services.

II. SYSTEM MODEL

We consider a coordinated-multipoint-enabled (CoMP-enabled) RAN slicing system for mIoT and bursty URLLC multiplexing service provision. From the viewpoint of infrastructure composition, the system mainly includes one baseband unit (BBU) pool and multiple RRHs connecting to the BBU via fronthaul links. From the perspective of network slicing, two types of inter-slices,

i.e., mMTC slices and URLLC slices, are exploited in this system with \mathcal{S}^I and \mathcal{S}^u denoting the mMTC slice set and URLLC slice set. We focus on the modelling of uplink IoT data transmission in mMTC slices and the modelling of downlink URLLC data transmission in URLLC slices. IoT devices (e.g., water meters and wearable e-health devices) are spatially distributed in \mathbb{R}^2 according to an independent homogeneous Poisson point process (PPP) $\Phi_s = \{u_{i,s}; s \in \mathcal{S}^I, i = 1, 2, \dots\}$ with intensity λ_s^I , where $u_{i,s}$ is the i -th IoT device's location in the s -th mMTC slice. There are N^u URLLC devices (e.g., remote-controlled robot sensors) that are randomly and evenly distributed in \mathbb{R}^2 . The RRHs are spatially distributed in \mathbb{R}^2 according to an independent PPP $\Phi_R = \{v_j; j = 1, 2, \dots\}$ with intensity λ_R , where v_j represents the location of the j -th RRH. The number and locations of IoT devices and RRHs will be fixed once deployed. Besides, each RRH is equipped with K antennas, and each device is equipped with a single antenna. The total network bandwidth W of the system is limited and shared by mMTC slices and URLLC slices. A flexible frequency division multiple access (FDMA) technique is utilized to achieve the inter-slice and intra-slice interference isolation [13]. In mMTC network slices, each IoT device is assumed to connect to its geographically closest RRH; thus, the cell area of each RRH constitutes a Voronoi tessellation. Just like [14], the co-channel inter-cell interference received by each RRH is assumed as a part of thermal noise mainly because of the intra-slice (or mMTC slice) interference isolation, the long-distance fading, and the severe wall penetration loss. Therefore, we focus on the analysis of the intra-cell interference in mMTC slices. In URLLC network slices, RRHs cooperate to transmit signals to a URLLC device to improve its signal-to-noise ratio (SNR).

Besides, in view of the architecture, the CoMP-enabled RAN slicing system consists of four parts including end devices, RAN coordinator (RAN-C), network slice management, and network providers. The system time is discretized and partitioned into time slots and minislots with a time slot consisting of T minislots. At the beginning of each time slot, the RAN-C will decide whether to accept or reject received network slice requests defined later after checking available resource information (e.g., physical resource blocks (PRBs)) and computing. If a slice request is accepted, network slice management will be responsible for creating or activating corresponding types of virtual slices and configuring RAN protocol stacks, the processes of which are time-consuming and usually in a timescale of minutes to hours. Next, if a slice request admission arrives, network providers will find the optimal servers and paths to deploy virtual network functions to satisfy the end-to-end QoS requirements of the slice. Meanwhile, at the beginning of each minislot, each active IoT device may try to connect to its associated RRH, and RRHs will generate cooperated

beamformers pointing at URLLC devices based on sensed channel coefficients.

Based on the above mentioned network slice concept, especially from the viewpoint of the slice's QoS requirement, we can define a mMTC slice request as follows.

Definition 1. A mMTC slice request is defined as a tuple $\{\lambda_s^I, \theta_s^{th}\}$ for any slice $s \in \mathcal{S}^I$, where θ_s^{th} is the signal-to-interference-plus-noise ratio (SINR) threshold for an RRH to successfully decode packets (including preamble packets and IoT data packets) sent from an IoT device in s .

In this paper, mMTC slice requests are assumed to be always accepted by the RAN-C. Although we give this assumption, it can be released by adding an slice access request indicator, e.g., $a_s \in \{0, 1\}$; if network resources are adequate and the RAN-C admits the slice request, we let $a_s = 1$; otherwise $a_s = 0$. RRHs will assign IoT devices to different slices according to the received SINR. The SINR threshold configured for all IoT devices in a slice is similar. For an IoT device in s , if it has the opportunity to send its endogenous arrival packets to the corresponding RRH, then it will randomly select a preamble (e.g., orthogonal Zadoff-tu sequences) from a BBU-maintained preamble pool and transmit the preamble to the RRH. Just like the literature [15], [16], although the whole connection establishment process usually follows an RA four-step procedure [17], we assume that a connection between the IoT device and the RRH is set up if the preamble can be successfully transmitted. In other words, the RA success probability is regarded as the probability of successfully transmitting a preamble in this paper.

Definition 2. A bursty URLLC slice request is defined as four tuples $\{I_s^u, D_s, \alpha, \beta\}$ for slice $s \in \mathcal{S}^u$, where I_s^u is the number of URLLC devices in s , D_s is the transmission latency requirement of each URLLC device in s , α and β are the packet blocking probability threshold and the codeword error decoding probability threshold of each URLLC device, respectively [11].

In this definition, URLLC devices are grouped into $|\mathcal{S}^u|$ clusters according to the transmission latency requirement of each device. As URLLC packets may arrive in burst and network resources allocated to URLLC slices may be inadequate, URLLC packets may experience blocking. The packet blocking probability threshold is then involved as a QoS requirement of URLLC slices. Besides, owing to the low latency requirement, URLLC packets should be immediately scheduled upon arrival; thus, URLLC slice requests should always be accepted by the RAN-C. Although we have this assumption, not all devices in URLLC slices can be served owing to limited network resources, as presented in detail in Section IV. We next analyze the RA success probability.

III. ANALYSIS OF RA SUCCESS PROBABILITY

A. Arrival, accumulation and departure of IoT packets

For a typical IoT device, we leverage a queue maintained in the device to capture the arrival, accumulation and departure of IoT packets. During minislot t , a Poisson distribution with intensity (or new arrivals) $\mu_{w,s}(t)$ is exploited to model the random, mutually independent endogenous packet arrivals in an IoT device in slice s . Once arrived, new packets will not be sent out immediately in general and will enter a queue in the IoT device, which is modelled as an $M/M/k$ queue with unlimited capacity, to wait for their scheduling. In the $M/M/k$ queue, packets will be scheduled according to the first-come, first-served (FCFS) basis. Besides, to facilitate the analysis of the queue evolution process, we consider the slotted-ALOHA RA protocol although there are many other RA protocols such as non-orthogonal and coded RA protocols. Owing to the RA behavior of the ALOHA protocol, new arrivals during t will only be counted at minislot $t + 1$. Thus, the accumulated number of packets $N_{a,s}(t)$ in the queue of a randomly selected IoT device in slice s during t is determined by the accumulated number of packets and the number of new arrivals during $t - 1$ and whether the preamble of the device can be successfully decoded by its associated RRH. The work in [16] presented a queue evolution model based on single packet transmission. We extend [16] to the case of multiple packets transmission, and (1) shows an evolution model of $N_{a,s}(t)$ for all $s \in \mathcal{S}^I$ with

$$N_{a,s}(t) = \begin{cases} 0, & t = 1 \\ [N_{w,s}(t-1) - \mathbb{1}(\text{RA succeeds})x_s]^+, & t = 2 \\ [N_{a,s}(t-1) + N_{w,s}(t-1) - \mathbb{1}(\text{RA succeeds})x_s]^+, & t \geq 3 \end{cases} \quad (1)$$

where $N_{w,s}(1)$ is the number of new arrivals in the 1st minislot, $\mathbb{1}(\cdot)$ is a function equaling to one if the corresponding RA succeeds; otherwise, $\mathbb{1}(\cdot) = 0$. $x_s = a \log_2(1 + \theta_s^{th})/L$ packets at the head of the queue will be popped out if $\mathbb{1}(\cdot) = 1$, where a is the size of the tone spacing in a single tone mode [2], L is the IoT packet length; otherwise, they will not. $[x]^+ = \max(x, 0)$.

At minislot t , based on the model in (1), for a randomly selected IoT device in slice $s \in \mathcal{S}^I$, the probability that its maintained queue is not empty can be defined as

$$P_{ne,s}(t) = \mathbb{P}\{N_{a,s}(t) > 0\} \quad (2)$$

(2) explicitly shows that new arrivals at t will not be sent out immediately, which is reflected in (1). (2) is significantly different from the work in [16], which defined the non-empty probability

$\mathcal{T}^m = \mathbb{P}\{N_{\text{Cum}}^m + N_{\text{New}}^m > 0\}$, where N_{Cum}^m was the number of accumulated packets, and N_{New}^m denoted the number of new arrivals in the m -th slot. This definition shows that new arrivals during the m -th slot have the probability of sending out immediately.

Next, we describe the packet departure process combined with a frame and minislot structure for the mIoT service. As mentioned above, partly due to the limitation on the frame and minislot structure, NB-IoT and LTE-M can only admit 50,000 devices. For NB-IoT, only one PRB with a bandwidth of 180 KHz in the frequency domain is allocated for the IoT service, and each physical channel occupies the whole PRB. For LTE-M, although the physical channels are time and frequency multiplexed, it only reserves six in-band PRBs with a total bandwidth of 1.08 MHz in the frequency domain for the IoT service. Thus, the frame and minislot structure for mIoT transmissions should be revisited if more RA requests from IoT devices want to be accepted.

Fig. 1 depicts a frame and minislot structure for mIoT transmissions. Although it depicts some essential channels, we do not discuss their correlations to the considered problem as the detailed research on the physical layer supporting the mIoT service is out of our scope. In this structure, both the frequency division multiplexing (FDM) scheme and code division multiplexing (CDM) scheme are leveraged to admit more IoT devices in a way of alleviating mutual device interference. Particularly, the FDM scheme can alleviate signal interference through orthogonal frequency allocation, and the CDM scheme mitigates the co-channel signal interference via reducing the cross-correlation of simultaneous transmissions. For a mIoT slice $s \in \mathcal{S}^I$, each subframe includes F_s orthogonal uplink physical RA channels (PRACHs). A single tone mode with a tone spacing of size of a MHz is adopted for each uplink PRACH, which indicates that each PRACH occupies a PRB. At the beginning of each minislot, an active IoT device, i.e., an IoT device whose queue is non-empty, will randomly choose a preamble from a set of non-dedicated RA preambles of size ξ and transmit the preamble through a randomly selected PRACH. For each preamble, it has an equal probability $1/\xi$ to be chosen by each IoT device. Similarly, each PRACH has an equal probability $1/F_s$ to be selected. Thus, the average number of IoT devices in mIoT slice $s \in \mathcal{S}^I$ choosing the same PRACH and the same preamble is $\lambda_s^I/\xi F_s$. Notably, a greater ξF_s may significantly reduce signal interference experienced at each RRH. Then, a question should be tackled: *How many PRBs should be reserved for mIoT transmissions?* To improve the resource utilization, the resource allocated to mIoT should be determined based on requirements of mIoT and other coexistence services. It motivates us to optimize the resources orchestrated for the mIoT service discussed in Section V, except for the RACH procedure analysis.

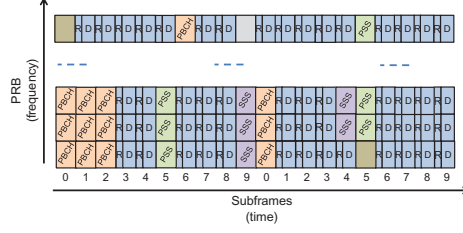


Fig. 1. The frame and minislot structure. 'R' and 'D' denote the resource block reserved for preamble and IoT data transmission. The preamble in 'R' also reflects the usage of a code division multiplexing scheme. PBCH, PSS and SSS represent the PRBs for physical broadcast channel, primary synchronization signal and secondary synchronization signal transmission, respectively.

B. Access control scheme

In a mMTC network slice, as the slotted-ALOHA protocol allows all active IoT devices to request for RA at the beginning of each minislot without checking channel statuses, IoT devices may simultaneously transmit preambles. It may incur severe slice congestion that may lower the RA success probabilities of IoT devices and degrade the system performance. Access control has been considered as an efficient proposal of alleviating congestion [18], and many access control schemes such as access class barring (ACB), power ramping and back-off schemes [16] have been proposed. As we aim at investigating the performance difference between a network slicing system without access control and with access control, we adopt the following two schemes [16]:

- 1) **Unrestricted scheme:** each active IoT device requests the RACH at the beginning of minislot t without access restriction;
- 2) **ACB scheme:** at the beginning of t , each active IoT device draws a random number $q \in [0, 1]$ and can request the RACH only when $q < P_{ACB}$, where P_{ACB} is an ACB factor determined by RRs based on the slice congestion condition.

With the introduced access control schemes, the probability that the RACH requests of a randomly selected IoT device in slice $s \in \mathcal{S}^I$ are not restricted at minislot t is defined as

$$P_{nr,s}(t) = \mathbb{P}\{\text{Unrestricted RACH requests}\} \quad (3)$$

For all $s \in \mathcal{S}^I$ at any minislot t , we have $P_{nr,s}(t) = 1$ for the unrestricted scheme and $P_{nr,s}(t) = P_{ACB}$ for the ACB scheme.

C. Derivation of RA success probability

For an RRH, if its received preamble SINR is no less than a preset SINR threshold, then the preamble is considered to be successfully transmitted. Just like [16], we do not investigate

the well-investigated preamble collision issue. Owing to the channel deep fading and severe co-channel interference, an IoT device may experience uplink preamble transmission outage. At minislot t , for a randomly selected active IoT device in $s \in \mathcal{S}^I$, its RA success probability is defined as

$$P_s(t) = \mathbb{P}\{SINR_s(t) \geq \theta_s^{th}\} \geq \pi_s \quad (4)$$

where $SINR_s(t)$ denotes the preamble SINR experienced at an RRH associating with the IoT device, π_s denotes a threshold of the required RA success probability.

We utilize a power-law path-loss model to calculate the path-loss between an IoT device and its RRH in mIoT slices and utilize a truncated channel inversion power control scheme to eliminate the ‘near-far’ effect. In this model, the IoT device’s transmit power decays at the rate of $r^{-\varphi}$ with r representing the propagation distance and φ denoting the path-loss exponent. In the power control scheme, IoT devices associated with the same RRH compensate for the path-loss to maintain that the average received signal power of an IoT device at the RRH equals to a threshold ρ_o . Without loss of generality, the cutoff threshold ρ_o is set to be the same for all RRHs, and we perform the analysis of RA success probability on an RRH located at the origin. According to Slivnyak’s theorem [19], the analysis holds for a generic RRH located at a generic location. For a randomly selected IoT device with a non-empty queue in $s \in \mathcal{S}^I$, the preamble SINR experienced at the RRH located at the origin can take the form

$$SINR_s(t) = \rho_o h_o / (\sigma^2 + \mathcal{I}_s(t)) \quad (5)$$

where σ^2 represents the noise power, $\mathcal{I}_s(t)$ denotes intra-cell interference received at the RRH, the useful signal power equals to $\rho_o h_o$ due to the truncated channel inversion power control [20] with h_o denoting the channel power gain between the IoT device and the RRH. Note that the channel power gain experienced at a generic RRH is related to the spatial locations of both the RRH and its associated IoT devices. Nevertheless, we drop the spatial indices for notation lightening. Besides, just like [20], all channel gains are assumed to be known and be independent of each other, independent of the spatial locations, symmetric and are identically distributed (i.i.d.). Considering both the particular IoT device deployment environment and the convenience of theoretical analysis, the Rayleigh fading is assumed, and the channel power gain h_o is assumed to be exponentially distributed with unit mean.

The intra-cell interference received at the origin RRH can take the following form

$$\mathcal{I}_s(t) = \sum_{m \in \mathcal{U}_s^I \setminus \{o\}} \mathbb{1}(p_m ||d_m||^{-\varphi} = \rho_o) \mathbb{1}(N_{a,s}(t) > 0) \mathbb{1}(f_m = f_o) \rho_o h_m \quad (6)$$

where u_s^I is the set of IoT devices connecting to the origin RRH in $s \in \mathcal{S}^I$, o is the randomly selected IoT device associated with the RRH at the origin, p_m denotes the transmit power of the m -th IoT device, $\|d_m\|$ is the distance between the m -th IoT device and the origin RRH, f_o denotes the preamble and channel chosen by the randomly selected IoT device, $f_o = f_m$ indicates that the randomly selected IoT device and the m -th IoT device select the same preamble and channel. The 1st $\mathbb{1}(\cdot)$ (from left to right) on the right-hand-side of (6) indicates that the received signal power of an interfering device at the origin RRH equals to ρ_o . The 2nd $\mathbb{1}(\cdot)$ denotes that the queue of an interfering device is non-empty. The 3rd $\mathbb{1}(\cdot)$ indicates that an interfering device selects the same preamble and channel as the randomly selected IoT device.

Then, for the randomly selected IoT device in $s \in \mathcal{S}^I$, we can rewrite (4) as follows

$$P_s(t) = \mathbb{P}\{h_o \geq \frac{\theta_s^{th}}{\rho_o}(\sigma^2 + \mathcal{I}_s(t))\} \stackrel{(a)}{=} \mathbb{E} \left[\exp \left\{ -\frac{\theta_s^{th}}{\rho_o}(\sigma^2 + \mathcal{I}_s(t)) \right\} \right] = e^{-\frac{\theta_s^{th}}{\rho_o}\sigma^2} \mathcal{L}_{\mathcal{I}_s(t)} \left(\frac{\theta_s^{th}}{\rho_o} \right) \quad (7)$$

where (a) follows from the full probability law over $\mathcal{I}_s(t)$, and $\mathcal{L}_{\mathcal{I}_s(t)}(\cdot)$ denotes the Laplace transform (LT) of the probability density function (PDF) of the random variable $\mathcal{I}_s(t)$. Note that the notation $\mathcal{L}_{\mathcal{I}_s(t)}(\cdot)$ is a terminology that is a slight abuse of subscript $\mathcal{I}_s(t)$.

The following lemma characterizes the LT of aggregate interference $\mathcal{I}_s(t)$. Although the work in [16] obtained an expression of the LT of aggregate interference $\mathcal{I}_{\text{Intra}}(t)$, we derive a significantly different result. In [16], the obtained $\mathcal{L}_{\mathcal{I}_{\text{Intra}}(t)}(\gamma_{th}/\rho)$ was a quasi-convex function over the system bandwidth allocated to IoT devices. In this paper, the obtained $\mathcal{L}_{\mathcal{I}_s(t)}(\theta_s^{th}/\rho_o)$ is the difference of two quasi-convex functions that significantly increases the difficulty of solving an optimization problem, which aims at improving IoT devices' total RA success probabilities and is presented in Section V.

Lemma 1. *For the origin RRH, based on the packet evolution model in (1), the LT of its received aggregate interference from active IoT devices associated with it is given by*

$$\mathcal{L}_{\mathcal{I}_s(t)}(\varpi_s) = \frac{1 + \varpi_s \rho_o}{(1 + \alpha_s \varpi_s \rho_o / (1 + \varpi_s \rho_o))^{3.5}} - \frac{1 + \varpi_s \rho_o}{(1 + \alpha_s)^{3.5}} \quad (8)$$

where $\varpi_s = \theta_s^{th}/\rho_o$, $\alpha_s = P_{nr,s}(t)P_{ne,s}(t)\lambda_s^I/(3.5\lambda_R\xi F_s)$.

Proof. See Appendix A. □

By substituting (8) into (7), we can obtain a mathematical expression of $P_s(t)$. The expression, however, is not in the closed-form as it is a function of $P_{ne,s}(t)$ the closed-form expression of which is not obtained. Next, we attempt to derive the closed-form expression of $P_{ne,s}(t)$.

D. Derivation of non-empty probability

According to the definition of non-empty probability, $P_{ne,s}(t)$ is correlated with $N_{a,s}(t)$. Thus, we theoretically analyze $P_{ne,s}(t)$ as the following.

From (1), we can observe that $N_{a,s}(1) = 0$ for all $s \in \mathcal{S}^I$; thus, at the 1st minislot, we have

$$P_{ne,s}^1 = \mathbb{P}\{N_{a,s}^1 > 0\} = 0 \quad (9)$$

where we write x^t instead of $x(t)$ to lighten the notation.

The following lemma presents the closed-form expression of the non-empty probability of a randomly selected IoT device served by the origin RRH when minislot $t > 1$. It is noteworthy that the derived expression of $P_{ne,s}(t)$ is completely different from that in [16] as this paper and [16] define different non-empty probabilities.

Lemma 2. *The number of accumulated packets of a randomly selected IoT device served by the origin RRH at minislot $t > 1$ may be approximately Poisson distributed. Therefore, based on the model in (1), for any mIoT slice $s \in \mathcal{S}^I$, we approximate the number of accumulated packets $N_{a,s}^t$ at t as a Poisson distribution with intensity $\mu_{a,s}^t$, which is given by*

$$\mu_{a,s}^t = \left[\mu_{w,s}^{t-1} + \mu_{a,s}^{t-1} - P_s^{t-1} \left(1 - e^{-\mu_{w,s}^{t-1} - \mu_{a,s}^{t-1}} \right) \right]^+ \quad (10)$$

Then, the probability that the queue of the device is non-empty at t can be written as

$$P_{ne,s}^t = 1 - e^{-\mu_{a,s}^t} \quad (11)$$

Proof. See Appendix B. □

Combined with (7), (8) and (11), the closed-form expression of $P_s(t)$ ($s \in \mathcal{S}^I$) can be obtained.

IV. RESOURCE ORCHESTRATION FOR BURSTY URLLC SLICES

In this section, we aim at addressing the following question: *How to orchestrate network resources of the CoMP-enabled RAN slicing system to satisfy the QoS requirements of bursty URLLC devices?*

During minislot t , a compound Poisson process, where arrivals happen in bursts (or batches, i.e., several arrivals can happen at the same instant) and the inter-batch times are independent and exponentially distributed [21], is utilized to model the number of bursty URLLC packets aggregated at each RRH. The intensity of the exponential distribution is set to be one batch. The number of new arrivals in each batch is subject to an independent homogeneous Poisson

distribution with intensity $\lambda = \{\lambda_s; s \in \mathcal{S}^u\}$, where λ_s denotes the intensity of new arrivals in a batch destined to devices belonging to URLLC slice s . Once arrived, new URLLC arrivals will enter a queue maintained by an RRH to be immediately scheduled. An $M/M/W^u$ queueing system with limited bandwidth W^u is exploited to model the queue. Without loss of any generality, we assume that each RRH maintains the same queue due to the exploration of cooperated transmission. In the queue, a packet destined to URLLC device $i \in \mathcal{I}_s^u$, $s \in \mathcal{S}^u$ will be allocated with a block of network bandwidth $\omega_{i,s}^u(t)$ for a period of time $d_s \leq D_s$ at minislot t . Owing to stochastic variations in the bursty packet arrival process, the limited bandwidth may not be enough to serve new arrivals occasionally. As such, URLLC packet blocking may happen. To reduce the probability of URLLC packet blocking, the PRB of the URLLC frame in the frequency domain should be narrowed while widening it in the time domain [22]. In this way, the number of concurrent transmissions will be increased, and the packet blocking probability is reduced. As the tolerable communication latency of a URLLC device $i \in \mathcal{I}_s^u$ in $s \in \mathcal{S}^u$ is D_s , we can scale up d_s and choose d_s and $\omega_{i,s}^u(t)$ at minislot t using the following equation

$$d_s = D_s \text{ and } \omega_{i,s}^u(t) = b_{i,s}^u(t)r_{i,s}^u(t)/(\kappa D_s) \quad (12)$$

where $r_{i,s}^u(t)$ denotes channel uses for transmitting a URLLC packet [22], κ is a constant reflecting the number of channel uses per unit time per unit bandwidth of FDMA frame structure and numerology, $b_{i,s}^u(t) \in \{0, 1\}$ is an indicator that indicates whether the device i in s can be served at minislot t . As mentioned above, because network resources are limited and shared by all network slices, not all URLLC devices can be guaranteed to be served at every minislot although the RAN-C will always accept the URLLC slice requests. If the QoS requirement of i in s is satisfied at t , then the device i can be served by the slice s , and we let $b_{i,s}^u(t) = 1$; otherwise, i cannot be served by s , and we let $b_{i,s}^u(t) = 0$. Certainly, we can adjust the slice priority weight introduced in the following section to guide the resource orchestration for the entire URLLC devices coverage.

Based on the result in (12), at minislot t , for a given $M/M/W^u$ queue with packet arrival intensity λ , the minimum upper bound of bandwidth orchestrated for URLLC slices with a packet blocking probability α and a packet queueing probability ς can be given by [11]

$$W^u(\mathbf{r}(t)) \leq \sum_{s \in \mathcal{S}^u} \sum_{i \in \mathcal{I}_s^u} \lambda_s b_{i,s}^u(t) \frac{r_{i,s}^u(t)}{\kappa} + \frac{\alpha - \varsigma \alpha}{\varsigma - \alpha} \sqrt{\frac{(\sum_{s \in \mathcal{S}^u} \sum_{i \in \mathcal{I}_s^u} b_{i,s}^u(t) \lambda_s^2 D_s^2) (\sum_{s \in \mathcal{S}^u} \sum_{i \in \mathcal{I}_s^u} \lambda_s b_{i,s}^u(t) \frac{r_{i,s}^u(t)^2}{\kappa^2 D_s})}{\min_{s \in \mathcal{S}^u} \{\lambda_s D_s\}}} \quad (13)$$

As (13) is correlated with the channel use $r_{i,s}^u(t)$, we next discuss how to obtain its expression. For any URLLC slice $s \in \mathcal{S}^u$, during minislot t , let $\mathbf{g}_{ij,s}(t) \in \mathbb{C}^K$ be the transmit beamformer pointing at the device i from the j -th RRH and $\mathbf{h}_{ij,s}(t) \in \mathbb{C}^K$ be the channel coefficient between the i -th URLLC device and the j -th RRH. The channel coefficient may change over minislots. However, it is assumed to be i.i.d. over each minislot and may not significantly change during each minislot. Then, the SNR received at device i in s at minislot t can be written as

$$SNR_{i,s}^u(t) = |\sum_{j \in \mathcal{J}} \mathbf{h}_{ij,s}^H(t) \mathbf{g}_{ij,s}(t)|^2 / \phi \sigma_{i,s}^2 \quad (14)$$

where $\mathcal{J} = \{1, 2, \dots, J\}$ denotes the set of deployed RRHs, $\phi > 1$ is an SNR loss coefficient owing to imperfect channel status information acquisition [23], $\sigma_{i,s}^2$ denotes the noise power. Just like [13], (14) does not include interference due to the usage of a flexible FDMA mechanism.

For URLLC transmission, we resort to the capacity analysis for a finite blocklength channel coding regime derived in [24] as the blocklength of a URLLC packet is short. For any device $i \in \mathcal{I}_s^u$, $s \in \mathcal{S}^u$, the number of transmitted information bits $L_{i,s}^u(t)$ at minislot t using $r_{i,s}^u(t)$ channel uses in an additive white Gaussian noise (AWGN) channel can be accurately correlated with the codeword¹ error decoding probability β according to the following equation [24]

$$L_{i,s}^u(t) \approx r_{i,s}^u(t) C(SNR_{i,s}^u(t)) - Q^{-1}(\beta) \sqrt{r_{i,s}^u(t) V(SNR_{i,s}^u(t))} \quad (15)$$

where $C(SNR_{i,s}^u(t)) = \log_2(1 + SNR_{i,s}^u(t))$, $V(SNR_{i,s}^u(t)) = \ln^2 2 \left(1 - \frac{1}{(1 + SNR_{i,s}^u(t))^2}\right)$ is the channel dispersion, and $Q(\cdot)$ is the Q -function.

The complicated expression of $V(SNR_{i,s}^u(t))$ in (15) significantly hinders the theoretical analysis of network resources orchestrated for URLLC slices. Fortunately, as $V(SNR_{i,s}^u(t))$ is upper-bounded by $\ln^2 2$, we can obtain the closed-form expression in (16) of the minimum upper bound of $r_{i,s}^u(t)$ with a codeword error decoding probability β by defining $x = \sqrt{r_{i,s}^u(t)}$ and solving a quadratic equation with respect to (w.r.t) x .

$$r_{i,s}^u(t) \leq \frac{L_{i,s}^u(t)}{C(SNR_{i,s}^u(t))} + \frac{(Q^{-1}(\beta))^2}{2(C(SNR_{i,s}^u(t)))^2} + \frac{(Q^{-1}(\beta))^2}{2(C(SNR_{i,s}^u(t)))^2} \sqrt{1 + \frac{4L_{i,s}^u(t)C(SNR_{i,s}^u(t))}{(Q^{-1}(\beta))^2}} \quad (16)$$

¹It is noteworthy that a URLLC packet will usually be coded before transmission and the generated codeword will be transmitted in the air interface such that the transmission reliability can be improved.

V. PROBLEM FORMULATION

Based on the above analysis, we next formulate the RAN slicing problem. In mMTC slices, each RRH may transmit feedback signals to its connected IoT devices for the connection establishment according to the RA four-step procedure [17]. Meanwhile, in URLLC slices, each RRH may transmit URLLC packets to URLLC devices. As the transmit power E_j ($j \in \mathcal{J}$) of each RRH is limited, we have the following transmit power constraint

$$\sum_{s \in \mathcal{S}^I} (1 + \alpha_g) \frac{\lambda_s^I}{\lambda_R} \hat{E}_j^I + \sum_{s \in \mathcal{S}^u} \sum_{i \in \mathcal{I}_s^u} b_{i,s}^u(t) \mathbf{g}_{ij,s}^H(t) \mathbf{g}_{ij,s}(t) \leq E_j \quad (17)$$

where \hat{E}_j^I is assumed to be a constant and denotes the transmit power of the j -th RRH for connecting to its associated IoT devices over downlink, α_g is a coefficient. As a PPP with intensity λ_s^I is utilized to model the distribution of IoT devices, the actual number of IoT devices may be greater than λ_s^I once deployed. As a result, the coefficient α_g is introduced to reserve transmit power for exceeded IoT devices.

In the RAN slicing system, as the total limited network bandwidth W will be shared by mMTC slices and URLLC slices, we have the following bandwidth constraint

$$\sum_{s \in \mathcal{S}^I} (1 + \alpha_g) \omega_s(\bar{t}) + W^u(\mathbf{r}(t)) \leq W \quad (18)$$

where $\omega_s(\bar{t})$ correlated with F_s by means of $F_s = \lfloor \omega_s(\bar{t})/a \rfloor$ denotes the bandwidth allocated to mMTC slice $s \in \mathcal{S}^I$. $\alpha_g \omega_s(\bar{t})$ denotes a block of reserved bandwidth for exceeded IoT devices.

In (18), F_s is an integer, and some integer variable recovery schemes [25] can be leveraged to obtain the suboptimal F_s . However, considering the high computational complexity of optimizing an integer variable and the utilization of the scheme of reserving additional bandwidth resources, we directly relax the integer variable into a continuous one, i.e., let $F_s = \omega_s(\bar{t})/a$. Without loss of any generality, we regard $\omega_s(\bar{t})$ as an independent variable below. Besides, as at least one PRB should be allocated to each type of mMTC slice $s \in \mathcal{S}^I$, we have

$$\omega_s(\bar{t}) \geq a \quad (19)$$

Owing to the exploration of mMTC and bursty URLLC service multiplexing, we should orchestrate network resources for all mMTC slices and URLLC slices to simultaneously maximize the slice utilities. For a mMTC slice $s \in \mathcal{S}^I$, its primary goal is to offload as many packets as possible from IoT devices. Thus, the number of accumulated packets in each IoT device should be kept at a low level. Considering that a great RA success probability of an IoT device will lead to a low number of accumulated packets, we define the mMTC slice utility as follows.

Definition 3. Over a time slot of duration T , the mIoT slice utility is defined as the time-average of RA success probabilities of IoT devices in all mIoT slices, which is given by

$$\bar{U}^I = \frac{1}{T} \sum_{t=1}^T U^I(t) = \frac{1}{T} \sum_{t=1}^T \tilde{P}(t) \quad (20)$$

where $\tilde{P}(t) = \sum_{s \in \mathcal{S}^I} \frac{\lambda_s^I P_s(t)}{\sum_{s \in \mathcal{S}^I} \lambda_s^I}$ with the numerator $\lambda_s^I P_s(t)$ represents the expected sum of RA success probabilities of IoT devices in slice $s \in \mathcal{S}^I$ and the denominator $\sum_{s \in \mathcal{S}^I} \lambda_s^I$ denoting a normalization coefficient.

In (20), $\lambda_s^I / \sum_{s \in \mathcal{S}^I} \lambda_s^I$ can be regarded as an intra-slice priority coefficient. A mIoT slice serving more IoT devices will be orchestrated with more network resources.

For a URLLC slice $s \in \mathcal{S}^u$, its primary objective is to maximize the slice gain reflected by the parameters in the slice request at a low cost. Therefore, we define an energy-efficient utility for URLLC slices, as presented below.

Definition 4. Over one time slot of duration T , the bursty URLLC slice utility is defined as the time-average energy efficiency for serving all URLLC devices, which is given by

$$\begin{aligned} \bar{U}^u &= \frac{1}{T} \sum_{t=1}^T U^u(t) = \frac{1}{T} \sum_{t=1}^T \sum_{s \in \mathcal{S}^u} U_s^u(D_s, \mathbf{g}_{ij,s}(t)) \\ &= \frac{1}{T} \sum_{t=1}^T \sum_{s \in \mathcal{S}^u} \sum_{i \in \mathcal{I}_s^u} \frac{b_{i,s}^u(t)}{1-e^{-D_s}} - \frac{\eta}{T} \sum_{t=1}^T \sum_{s \in \mathcal{S}^u} \sum_{j \in \mathcal{J}} \sum_{i \in \mathcal{I}_s^u} b_{i,s}^u(t) \mathbf{g}_{ij,s}^H(t) \mathbf{g}_{ij,s}(t) \end{aligned} \quad (21)$$

where η is an energy efficiency coefficient indicating a tradeoff between the URLLC slice gain and the RRH energy consumption.

In (21), we characterize the slice gain by $\frac{1}{T} \sum_{t=1}^T \sum_{s \in \mathcal{S}^u} \sum_{i \in \mathcal{I}_s^u} \frac{b_{i,s}^u(t)}{1-e^{-D_s}}$ as it reflects the latency requirements of bursty URLLC slices. Then, during a time slot, the original RAN slicing problem for mIoT and URLLC service multiplexing can be formulated as follows.

$$\underset{\{b_{i,s}^u(t), \omega_s(\bar{t}), \mathbf{g}_{ij,s}(t)\}}{\text{maximize}} \quad \bar{U}^I + \tilde{\rho} \bar{U}^u \quad (22a)$$

$$\text{s.t. } b_{i,s}^u(t) \in \{0, 1\}, \forall s \in \mathcal{S}^u, i \in \mathcal{I}_s^u \quad (22b)$$

$$\text{constraints (4), (17) – (19) are satisfied.} \quad (22c)$$

where $\tilde{\rho}$ is an inter-slice priority coefficient reflecting the priority of orchestrating network resources for mIoT slices and URLLC slices.

The solution of (22) is quite challenging mainly because i) **indeterministic objective function:** (22) should be optimized at the beginning of the 1st minislot. The time-averaged objective

function of (22) can only be exactly computed according to the future channel information. Therefore, the value of the objective function is indeterministic at the beginning of the 1st minislot; ii) **two timescale issue**: the creation of a network slice is performed at a timescale of time slot. Thus, the variable $\omega_s(\bar{t})$ should be determined at the beginning of the time slot \bar{t} and kept unchanged over the whole time slot. The channel, however, is time-varying. As a result, the beamformer $\mathbf{g}_{ij,s}(t)$ should be optimized at each minislot t . In summary, the variables in (22) should be optimized at two different timescales; iii) **thorny optimization problem**: at each minislot t , the constraint (4) is non-convex over $\omega_s(\bar{t})$, and the constraints (17), (18) are non-convex over $\mathbf{g}_{ij,s}(t)$, which together lead to a non-convex problem.

Next, we attempt to tackle these challenges by exploiting of an SAA technique [26], an ADMM method [27], a relaxation scheme and an approximation scheme.

VI. PROBLEM SOLUTION WITH SYSTEM GENERATED CHANNEL

A. Sample average approximation and alternating direction method of multipliers

As mMTC slices and URLLC slices share the network resources, both \bar{U}^I and \bar{U}^u may be determined by channel coefficients experienced by URLLC slices. At each minislot t , due to the i.i.d. assumption on the channel coefficients of URLLC slices, we have

$$\frac{1}{T} \sum_{t=1}^T U^I(t) + \frac{1}{T} \sum_{t=1}^T \tilde{\rho} U^u(t) \approx \mathbb{E}_{\hat{\mathbf{h}}} [\hat{U}^I + \tilde{\rho} \hat{U}^u] \quad (23)$$

where $\hat{\mathbf{h}}$ is the channel samples of URLLC slices collected at the beginning of the time slot \bar{t} .

Given a collection of channel samples $\{\mathbf{h}_m\}$ with $\mathbf{h}_m = [\mathbf{h}_{11,1m}; \dots; \mathbf{h}_{1J,sm}; \dots; \mathbf{h}_{N^u J, |S^u| m}]$ and $m \in \mathcal{M} = \{1, \dots, M\}$. For notation lightening, we write x_m instead of $x(m)$ that represents a variable corresponding to the channel sample \mathbf{h}_m . Just like [11], as constraints (22b) and (22c) construct a nonempty compact set, the conclusion of Proposition 5.1 in [11] is applicable to this paper by exploiting the SAA technique. The conclusion indicates that if the number of channel samples M is reasonably large, then $\frac{1}{M} \sum_{m=1}^M U_m^I + \frac{\tilde{\rho}}{M} \sum_{m=1}^M U_m^u$ converges to $\mathbb{E}_{\hat{\mathbf{h}}} [\hat{U}^I + \hat{U}^u]$ uniformly on the nonempty compact set almost surely. In other words, the SAA technique enables us to use the channel samples collected at the beginning of a time slot to approximate the unknown channel coefficients over the time slot.

Recall that the variable $\omega_s(\bar{t})$ will be kept unchanged over the time slot \bar{t} and the beamformer $\mathbf{g}_{ij,s}(t)$ should be calculated at each minislot t , we can further consider (22) as a global consensus problem [27], which can be effectively mitigated by an ADMM method. In (22), $\omega_s(\bar{t})$ is a global

consensus variable that should be maintained in consensus for all \mathbf{h}_m ($m \in \mathcal{M}$), and $\mathbf{g}_{ij,sm}$ that is calculated based on \mathbf{h}_m is a local variable. The fundamental principle of ADMM is to impose augmented penalty terms characterizing global consensus constraints on the objective function of an optimization problem. In this way, the local variables can be driven into the global consensus while still attempting to maximize the objective function. Let $\mathbf{G}_{i,sm} = \mathbf{g}_{i,sm} \mathbf{g}_{i,sm}^H \in \mathbb{R}^{JK \times JK}$, $\mathbf{H}_{i,sm} = \mathbf{h}_{i,sm} \mathbf{h}_{i,sm}^H \in \mathbb{R}^{JK \times JK}$, where $\mathbf{g}_{i,sm} = [\mathbf{g}_{i1,sm}; \dots; \mathbf{g}_{iJ,sm}] \in \mathbb{C}^{JK \times 1}$ and $\mathbf{h}_{i,sm} = [\mathbf{h}_{i1,sm}; \dots; \mathbf{h}_{iJ,sm}] \in \mathbb{C}^{JK \times 1}$. By applying the property [28] $\mathbf{G}_{i,sm} = \mathbf{g}_{i,sm} \mathbf{g}_{i,sm}^H \Leftrightarrow \mathbf{G}_{i,sm} \succeq 0$, $\text{rank}(\mathbf{G}_{i,sm}) \leq 1$ and utilizing the conclusions of SAA and ADMM, we can approximate (22) as the following problem at the beginning of the time slot \bar{t} .

$$\underset{\{\omega_{sm}, \omega_s(\bar{t}), b_{i,sm}^u, \mathbf{G}_{i,sm}\}}{\text{minimize}} \sum_{m=1}^M \left[-\frac{U_m^I}{M} - \frac{\tilde{\rho} U_m^u}{M} \right] + \underbrace{\sum_{m=1}^M \sum_{s \in \mathcal{S}^I} \left[\psi_{sm} (\omega_{sm} - \omega_s(\bar{t})) + \frac{\mu}{2} \|\omega_{sm} - \omega_s(\bar{t})\|_2^2 \right]}_{\text{augmented penalty terms}} \quad (24a)$$

$$\text{s.t. } P_{sm} \geq \pi_s, \forall s \in \mathcal{S}, m \in \mathcal{M} \quad (24b)$$

$$\sum_{s \in \mathcal{S}^I} (1 + \alpha_g) \frac{\lambda_s^I}{\lambda_R} \hat{E}_j^I + \sum_{s \in \mathcal{S}^u} \sum_{i \in \mathcal{I}_s^u} b_{i,sm}^u \text{tr}(\mathbf{Z}_j \mathbf{G}_{i,sm}) \leq E_j, \forall j \in \mathcal{J}, m \in \mathcal{M} \quad (24c)$$

$$\sum_{s \in \mathcal{S}^I} (1 + \alpha_g) \omega_s(\bar{t}) + W^u(\mathbf{r}_m) \leq W, m \in \mathcal{M} \quad (24d)$$

$$\mathbf{G}_{i,sm} \succeq 0, \forall s \in \mathcal{S}^u, i \in \mathcal{I}_s^u, m \in \mathcal{M} \quad (24e)$$

$$\text{rank}(\mathbf{G}_{i,sm}) \leq 1, \forall s \in \mathcal{S}^u, i \in \mathcal{I}_s^u, m \in \mathcal{M} \quad (24f)$$

$$b_{i,sm}^u \in \{0, 1\}, \forall s \in \mathcal{S}^u, i \in \mathcal{I}_s^u, m \in \mathcal{M} \quad (24g)$$

$$\text{constraint (19) is satisfied} \quad (24h)$$

where ψ_{sm} is the Lagrangian multiplier, μ is a penalty coefficient, \mathbf{Z}_j is a square matrix with $J \times J$ blocks, and each block in \mathbf{Z}_j is a $K \times K$ matrix. In \mathbf{Z}_j , the block in the j -th row and j -th column is a $K \times K$ identity matrix, and all other blocks are zero matrices.

(22) is now reduced to a deterministic single timescale problem (24). What is more, (24) can be split into M separate problems that can be optimized in parallel as its objective function is separable. Thus, the following ADMM-based framework from (25) to (27) can be exploited to mitigate (24).

$$\left\{ \omega_{sm}^{(k+1)}, b_{i,sm}^{u(k+1)}, \mathbf{G}_{i,sm}^{(k+1)} \right\} = \underset{\{\omega_{sm}, b_{i,sm}^u, \mathbf{G}_{i,sm}\}}{\text{argmin}} \bar{\mathcal{L}}(\omega_{sm}, \mathbf{G}_{i,sm}) \quad (25a)$$

$$\text{s.t. for the } m\text{-th sample, (24b) - (24g) are satisfied} \quad (25b)$$

for the m -th sample, $\omega_{sm} \geq a$, $\forall s \in \mathcal{S}^I$ (25c)

$$\omega_s^{(k+1)}(\bar{t}) = \sum_{m=1}^M (\omega_{sm}^{(k+1)} + \psi_{sm}^{(k)}/\mu)/M, \quad \forall s \in \mathcal{S}^I \quad (26)$$

$$\psi_{sm}^{(k+1)} = \psi_{sm}^{(k)} + \mu (\omega_{sm}^{(k+1)} - \omega_s^{(k+1)}(\bar{t})), \quad \forall s \in \mathcal{S}^I \quad (27)$$

where the augmented partial Lagrangian function

$$\bar{\mathcal{L}}(\omega_{sm}, \mathbf{G}_{i,sm}) = -\frac{U_m^{I(k)}}{M} - \frac{\tilde{\rho}U_m^{u(k)}}{M} + \sum_{s \in \mathcal{S}^I} \left[\psi_{sm}^{(k)} (\omega_{sm} - \omega_s^{(k)}(\bar{t})) + \frac{\mu}{2} \|\omega_{sm} - \omega_s^{(k)}(\bar{t})\|_2^2 \right] \quad (28)$$

This ADMM-based framework can be executed on multiple processors. Each processor is responsible for optimizing (25) and calculating (27) with a global value as an input. (26) is centrally updated in such a way that local variables converge to the global value, which is the solution of (24). Unfortunately, (25) is a mixed-integer non-convex optimization problem as there are zero-one variables, continuous variables and non-convex constraints in (25). As a result, the optimization of (25) is quite difficult. We next discuss how to handle this hard problem.

B. Alternative optimization

In this subsection, we exploit an alternative optimization scheme to handle the mixed-integer non-convex optimization problem. Specifically, we first assume that continuous variables are known and attempt to mitigate a zero-one optimization problem. Given the zero-one variables, we then try to optimize a non-convex optimization problem. The process is alternatively conducted until convergence.

1) *URLLC device associations*: Given continuous variables $\{\mathbf{G}_{i,sm}^{(k)}, \omega_{sm}^{(k)}\}$ at the k -th iteration, the association problem of URLLC devices in URLLC slices can take the following form

$$\{b_{i,sm}^{u(k+1)}\} = \operatorname{argmin}_{\{b_{i,sm}^u\}} -\tilde{\rho}U_m^{u(k)}/M \quad (29a)$$

$$\text{s.t. for } m, (24c), (24d), (24g) \text{ are satisfied.} \quad (29b)$$

This problem is non-linear and hard to be handled. In theory, an exhaustive algorithm can obtain the optimal solution of (29). The computation complexity of this algorithm is $O(2^{N^u})$ that may be impractical in implementation. Therefore, a greedy scheme of the computational complexity $O(N^u)$, which is summarized as the following, is proposed to obtain $\{b_{i,sm}^{u(k+1)}\}$.

- a) initialize two device sets, i.e., candidate device set $\mathcal{I}^{u-} = \mathcal{I}^u$, association device set $\mathcal{I}^{u+} = \emptyset$.
- b) select the device that maximizes $\tilde{\rho}U_m^{u(k)}/M$ from \mathcal{I}^{u-} , remove it from \mathcal{I}^{u-} , and add it to \mathcal{I}^{u+} .

Given \mathcal{I}^{u+} , check the feasibility of (29). If (29) is feasible, then accept the device; otherwise, remove the device from \mathcal{I}^{u+} . Continue till $\mathcal{I}^{u-} = \emptyset$.

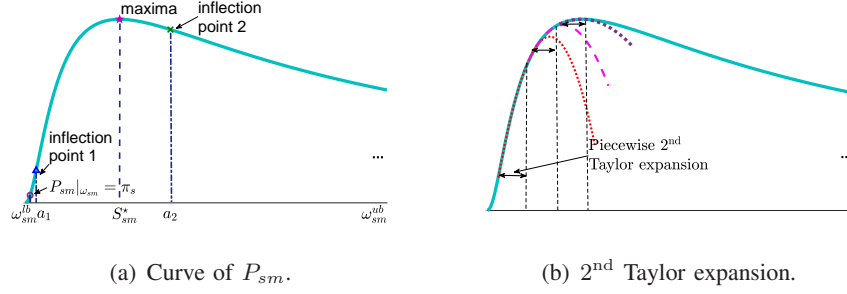


Fig. 2. Curve of P_{sm} and its 2nd Taylor expansion.

2) *Joint bandwidth and beamforming optimization:* Given the obtained $b_{i,sm}^{u(k+1)}$, (24) will be reduced to the following joint bandwidth and beamforming problem.

$$\left\{ \omega_{sm}^{(k+1)}, \mathbf{G}_{i,sm}^{(k+1)} \right\} = \underset{\{\omega_{sm}, \mathbf{G}_{i,sm}\}}{\operatorname{argmin}} \bar{\mathcal{L}}(\omega_{sm}, \mathbf{G}_{i,sm}) \quad (30a)$$

$$\text{s.t. for } m, (24b) - (24f), (25c) \text{ are satisfied.} \quad (30b)$$

In (30), the low-rank constraint (24f) is non-convex, and its objective function is not convex and even not quasi-convex w.r.t. ω_{sm} , the tackling of which is quite tricky. To tackle the non-convex low-rank constraint (24e), we resort to the SDR technique. The primary procedures of SDR are i) directly drop the low-rank constraint; ii) solve the optimization problem without the low-rank constraint to obtain the solution; iii) if the obtained solution is not rank-one, then some manipulations such as randomization/scale [29] are needed to perform on it to impose the low-rank constraint; otherwise, its principal component is the optimal solution to (30).

For the tricky objective function, we are reminded of the art of dealing with a non-convex function, i.e., study the structure of the function if it is non-convex. A crucial observation is that P_{sm} is quasi-concave w.r.t. ω_{sm} although the objective function is not quasi-convex w.r.t. ω_{sm} . Therefore, we resort to the Taylor expansion to approximate the tricky objection function.

The following analysis is based on two facts **Fact 1**: the value of the objective function of (30) is mainly determined by that of $\tilde{P}_m^{(k)}$ (or $U_m^{I(k)}$); **Fact 2**: the solution ω_{sm} maximizing $\tilde{P}_m^{(k)}$ must locate in the range of $[\hat{\omega}_{sm}^{lb}, S_{sm}^*] \forall s, m$ shown in Fig. 2, where $\hat{\omega}_{sm}^{lb} = \max\{\omega_{sm}^{lb}, a\}$ with ω_{sm}^{lb} denoting the lower bound of ω_{sm} satisfying the constraint (24b), S_{sm}^* is the ω_{sm} maximizing P_{sm} , and the notation $P_{sm}|_{\omega_{sm}}$ is utilized to explicitly indicate that P_{sm} is a function of ω_{sm} .

Fact 1 holds because the linear terms w.r.t. ω_{sm} will donate little to the objective function as the consensus constraint is active. Besides, the quadratic terms pull local values towards the consensus; thus, they will also donate little to the objective function. Fact 2 holds because

the total bandwidth is limited and shared. For example, given a value $\omega_{sm,2} \in [S_{sm}^* + \delta_\omega, W]$ with δ_ω being a small positive constant, there must exist a value $\omega_{sm,1} \in [\hat{\omega}_{sm}^{lb}, S_{sm}^*]$ such that $P_{sm}|_{\omega_{sm,1}} = P_{sm}|_{\omega_{sm,2}}$. Thus, a small ω_{sm} will be preferred as it indicates that more bandwidth can be allocated to URLLC slices to further improve the objective function.

For all $s \in \mathcal{S}^I$, it can be proved that P_{sm} is concave in the interval $(a_1, a_2]$ by evaluating the second-order derivative of P_{sm} . Thus, we can use the 2nd Taylor expansion to approximate P_{sm} in this interval. Considering that P_{sm} is convex in the interval $[\hat{\omega}_{sm}^{lb}, a_1]$, the 1st Taylor expansion is always used to obtain the lower bound of P_{sm} . However, this interval is usually rather narrow, and the value of P_{sm} in this interval is much lower than that in the interval $(a_1, a_2]$. What is more, the error bound of the 1st Taylor expansion is greater than that of the 2nd expansion. Therefore, we explore the 2nd Taylor expansion to approximate P_{sm} in the interval $[\hat{\omega}_{sm}^{lb}, a_2]$. Fig. 2(b) shows an example of the 2nd Taylor expansion of P_{sm} . Given a local point $\omega_m^{(k,q)}$ at the q -th iteration, the Taylor expansion of $\tilde{P}_m^{(k)}$ at the local point can be given by

$$-\tilde{P}_m^{(k)} \approx -\tilde{P}_m^{(k,q)} - \nabla \tilde{P}_m^{(k,q)} (\omega_m - \omega_m^{(k,q)})^T - \frac{1}{2} (\omega_m - \omega_m^{(k,q)}) H(\omega_m^{(k,q)}) (\omega_m - \omega_m^{(k,q)})^T - R_2(\omega_m) \quad (31)$$

where $\omega_m = [\omega_{1m}, \dots, \omega_{|\mathcal{S}^I|_m}]$, $\nabla \tilde{P}_m^{(k,q)}$ is the gradient of $\tilde{P}_m^{(k)}$ over ω_m at the local point $\omega_m^{(k,q)}$ with

$$\frac{\partial P_{sm}^{(k)}}{\partial \omega_{sm}^{(k,q)}} = \frac{\lambda_s^I (1 + \varpi_s \rho_o) e^{-\varpi_s \sigma^2}}{\sum_{s \in \mathcal{S}^I} \lambda_s^I} \left[\frac{3.5 y_{sm} z_s \omega_{sm}^{2.5(k,q)}}{(y_{sm} z_s + \omega_{sm}^{(k,q)})^{4.5}} - \frac{3.5 y_{sm} \omega_{sm}^{2.5(k,q)}}{(y_{sm} + \omega_{sm}^{(k,q)})^{4.5}} \right] \quad (32)$$

and $H(\omega_m^{(k,q)})$ is a Hessian matrix with

$$\frac{\partial^2 P_{sm}^{(k)}}{\partial \omega_{sm}^{2(k,q)}} = \frac{\lambda_s^I (1 + \varpi_s \rho_o) e^{-\varpi_s \sigma^2}}{\sum_{s \in \mathcal{S}^I} \lambda_s^I} \left[\frac{15.75 y_{sm}^2 z_s^2 \omega_{sm}^{1.5(k,q)}}{(y_{sm} z_s + \omega_{sm}^{(k,q)})^{5.5}} - \frac{7 y_{sm} z_s \omega_{sm}^{1.5(k,q)}}{(y_{sm} z_s + \omega_{sm}^{(k,q)})^{4.5}} \right] + \frac{\lambda_s^I (1 + \varpi_s \rho_o) e^{-\varpi_s \sigma^2}}{\sum_{s \in \mathcal{S}^I} \lambda_s^I} \left[\frac{7 y_{sm} \omega_{sm}^{1.5(k,q)}}{(y_{sm} + \omega_{sm}^{(k,q)})^{4.5}} - \frac{15.75 y_{sm}^2 \omega_{sm}^{1.5(k,q)}}{(y_{sm} + \omega_{sm}^{(k,q)})^{5.5}} \right] \quad (33)$$

$$\frac{\partial^2 P_{sm}^{(k)}}{\partial \omega_{sm}^{(k,q)} \partial \omega_{s'm}^{(k,q)}} = 0, \forall s \neq s' \quad (34)$$

$y_{sm} = a P_{nr,sm} P_{ne,sm} \lambda_s^I / (3.5 \lambda_R)$, $z_s = \theta_s^{th} / (1 + \theta_s^{th})$. Besides, we write $\omega_{sm}^{2.5(k,q)}$ rather than $(\omega_{sm}^{(k,q)})^{2.5}$ for lightening the notation.

Lemma 3. Let the function $\tilde{P}_m^{(k)} : \mathbb{R}^{|\mathcal{S}^I|} \rightarrow \mathbb{R}$ be three times differentiable in a given interval $[\hat{\omega}_{sm}^{lb}, S_{sm}^*]$ for all $s \in \mathcal{S}^I$, then the error bound of 2nd degree Taylor expansion of $\tilde{P}_m^{(k)}$ at the local point $\omega_m^{(k,q)}$ with $\omega_{sm}^{(k,q)} \in [\hat{\omega}_{sm}^{lb}, S_{sm}^*]$ is given by

$$R_2(\omega_m) = \frac{1}{3!} \left[\sum_{s \in \mathcal{S}^I} (\omega_{sm} - \omega_{sm}^{(k,q)}) \frac{\partial}{\partial \omega_{sm}^{(k,q)}} \right]^3 \max \left\{ \tilde{P}_m^{(k)}|_{\hat{\omega}_m^{lb}}, \tilde{P}_m^{(k)}|_{S_m^*} \right\} \quad (35)$$

where $\hat{\omega}_m^{lb} = [\hat{\omega}_{1m}^{lb}, \dots, \hat{\omega}_{|S^I|_m}^{lb}]$ and $\mathbf{S}_m^* = [S_{1m}^*, \dots, S_{|S^I|_m}^*]$.

Proof. See Appendix C. \square

After conducting the 2nd Taylor approximation, the objective function becomes a convex function. Although the constraint (24b) is $P_{sm} \forall s, m$ related, we need not to conduct the Taylor approximation on (24b) as P_{sm} is quasi-concave and unimodal. In fact, the probability constraint (24b) and (25c) are equivalent to the following inequality

$$\hat{\omega}_{sm}^{lb} \leq \omega_{sm} \leq \omega_{sm}^{ub} \quad (36)$$

where $\omega_{sm}^{ub} \leq W$ represents the upper bound of ω_{sm} satisfying (24b).

Next, a low-complexity bisection-search-based scheme, the main procedures of which are described below, is developed to obtain ω_{sm}^{lb} , S_{sm}^* , and ω_{sm}^{ub} : a) let the function $Q_{sm} = P_{sm} - \pi_s$. Perform the bisection search method [30] on $Q_{sm} = 0$ to obtain ω_{sm}^{lb} and ω_{sm}^{ub} that are the two zero points of Q_{sm} ; b) with the obtained ω_{sm}^{lb} and ω_{sm}^{ub} , find the maximum value S_{sm}^* of P_{sm} using the bisection search method again.

According to the above analysis, at the q -th iteration, we can rewrite (30) as

$$\left\{ \omega_{sm}^{(k+1,q+1)}, \mathbf{G}_{i,sm}^{(k+1,q+1)} \right\} = \underset{\{\omega_{sm}, \mathbf{G}_{i,sm}\}}{\operatorname{argmin}} \bar{\mathcal{L}}^{(q)}(\omega_{sm}, \mathbf{G}_{i,sm}) \quad (37a)$$

$$\text{s.t. for } m, (24c) - (24e), (36) \text{ are satisfied.} \quad (37b)$$

where $\bar{\mathcal{L}}^{(q)}(\omega_{sm}, \mathbf{G}_{i,sm}) = -\frac{1}{M} \tilde{P}_m^{(k)} - \frac{\bar{\rho} U_m^{u(k)}}{M} + \sum_{s \in S^I} \left[\psi_{sm}^{(k,q)}(\omega_{sm} - \omega_s^{(k,q)}(\bar{t})) + \frac{\mu}{2} \|\omega_{sm} - \omega_s^{(k,q)}(\bar{t})\|_2^2 \right]$.

In (37), the objective function is convex, (24c) is affine, and the constraint (24d) can be proved to be convex w.r.t. both ω_{sm} and $\mathbf{G}_{i,sm}$ [11]. Therefore, (37) is a convex problem that can be effectively mitigated by some standard convex optimization tools such as CVX and MOSEK.

Then we can summarize the main steps of mitigating the problem (24) in Algorithm 1.

Lemma 4. For all $i \in \mathcal{I}_s^u$, $s \in \mathcal{S}^u$, and $m \in \mathcal{M}$, the obtained power matrix $\mathbf{G}_{i,sm}^{(k,q)}$ by Algorithm 1 at the (k, q) -th iteration satisfies the low-rank constraint, i.e., the SDR for the power matrix utilized in Algorithm 1 is tight.

Proof. See Appendix D. \square

VII. OPTIMIZATION OF BEAMFORMING WITH SYSTEM SENSED CHANNELS

In Section VI, we obtained a family of global consensus variables $\{\omega_s(\bar{t})\}$ with the system generated channel samples. The time-varying actual channels may require the re-optimization of

Algorithm 1 ADMM-based bandwidth allocation algorithm

- 1: **Initialization:** Randomly initialize $\mathbf{G}_{i,s}^{(0,0)}$, $\{\omega_s^{(0,0)}\}$, let $k_{\max} = 250$, $q_{\max} = 250$, $q = 0$, $k = 0$, and generate channel samples $\{\mathbf{H}_{i,sm}\}$.
 - 2: **repeat**
 - 3: **repeat**
 - 4: Given $\mathbf{G}_{i,sm}^{(k,q)}$, $\omega_{sm}^{(k,q)}$, call the greedy scheme to obtain $b_{i,sm}^{u(k,q+1)}$.
 - 5: Optimize (37) with obtained $b_{i,sm}^{u(k,q+1)}$ to achieve $\mathbf{G}_{i,sm}^{(k,q+1)}$ and $\omega_{sm}^{(k,q+1)}$. Update $q = q + 1$.
 - 6: **until** Convergence or reach at the maximum iteration times q_{\max} .
 - 7: Let $\omega_{sm}^{(k+1,q+1)} = \omega_{sm}^{(k,q+1)}$, update $\psi_{sm}^{(k+1)}$, $\omega_s^{(k+1)}(\bar{t})$ using (27), (26), and update $k = k + 1$.
 - 8: **until** Convergence or reach at the maximum iteration times k_{\max} .
-

beamformers and device associations at each minislot. According to system sensed channels at each minislot, we next discuss how to calculate beamforms and device associations.

At each minislot t , given the global consensus variables $\{\omega_s(\bar{t})\}$, the original problem (22) will be reduced to the following problem

$$\begin{aligned} & \underset{\{b_{i,s}^u(t), \mathbf{G}_{i,s}(t)\}}{\text{maximize}} \quad \tilde{\rho} U^u(t) \end{aligned} \quad (38a)$$

$$\text{s.t. constraints (17), (18), (22b) are satisfied.} \quad (38b)$$

In (38), the channels are system sensed ones at t . According to the convexity analysis in Section VI, (38) is a mixed-integer non-convex programming problem with positive semidefinite matrices, which is hard to be mitigated. Therefore, the alternative optimization scheme presented in subsection VI-B can be leveraged to achieve the solutions $b_{i,s}^u(t)$ and $\mathbf{G}_{i,s}(t)$ of (38). Lemma 4 indicates that the achieved $\text{rank}(\mathbf{G}_{i,s}(t)) \leq 1$. Thus, we can obtain the beamformers $\mathbf{g}_{i,s}(t)$ by performing the eigendecomposition on $\mathbf{G}_{i,s}(t)$. To sum up, over a time slot \bar{t} , the slice resource optimization algorithm designed for the RAN slicing system can be summarized in Algorithm 2.

VIII. SIMULATION RESULTS

A. Comparison algorithms and parameter setting

We compare the following three algorithms to verify the effectiveness of the proposed algorithm and to explain the impact of access control schemes on the RAN system performance

Algorithm 2 slice resource optimization algorithm, SRO

- 1: **Initialization:** $\{\mathbf{H}_{i,s}(t)\}$, $\forall i \in \mathcal{I}^u$, $s \in \mathcal{S}^u$, and let $P_s^1 \in [0, 1]$, $\mu_{a,s}^1 = 0$, $\forall s \in \mathcal{S}^I$.
 - 2: Call Algorithm 1 to obtain $\{\omega_s(\bar{t})\}$ for all $s \in \mathcal{S}^I$.
 - 3: **for** $t = 1 : T$ **do**
 - 4: Given $\{\omega_s(\bar{t})\}$, mitigate (38) by exploiting the alternative optimization scheme to obtain beamformers $\{\mathbf{g}_{i,s}(t)\}$ and URLLC device associations $b_{i,s}^u(t)$ for all $i \in \mathcal{I}_s^u$, $s \in \mathcal{S}^u$.
 - 5: **end for**
-

intuitively i) SRO algorithm that adopts the unrestricted access control scheme; ii) SRO-ACB_I algorithm that utilizes the ACB access control scheme with $P_{ACB} = 0.9$; iii) SRO-ACB_{II} algorithm that adopts the ACB access control scheme with $P_{ACB} = 0.5$. However, we do not discuss how to select access control schemes and their parameters such as P_{ACB} . We focus on investigating whether the conclusions of adopting access control schemes in an individual IoT service system can still hold in the case of service multiplexing.

The parameter setting is as follows: RRHs and IoT devices are deployed following independent PPPs in a one km² area. URLLC devices are randomly and uniformly distributed in this area. There are three mMTC slices and two URLLC slices in the RAN slicing system. For the mMTC slices, set $\mu_{w,s}(t) = [1.5, 1.0, 0.5]$, $\pi_s = 0.5$, $\forall s, t$, $\varphi = 4$, $L = 2000$ bits, $\sigma^2 = -90$ dBm, $\rho_o = -90$ dBm, $\hat{E}_j^I = 0.03$ mW, $\lambda_R = 3$ RRHs/km², $\lambda_s^I = 18000$ IoT devices/km², $\forall s$, $a = 0.18$ MHz, the queue serving rate $\gamma_s^{th} = a \log_2(1 + \theta_s^{th})$, $\{\gamma_s^{th}\} = \{5.8, 4.35, 2.9\}$ Kbits/minislot. For the URLLC slices, the transmit antenna gain at each RRH is set to be 5 dB, and a log-normal shadowing path-loss model is used to simulate the path-loss between an RRH and a URLLC device with the log-normal shadowing parameter being 10 dB. A path-loss is computed by $h(\text{dB}) = 128.1 + 37.6 \log_{10} d$, where d (in km) is the distance between a device and an RRH. Let $L_{i,s}^u = 160$ bits, $\sigma_{i,s}^2 = -100$ dBm, $\lambda_s = \lambda = 0.1$ packets/minislot, $\forall i, s$, $\{I_s^u\} = \{3, 5\}$ devices, and $\{D_s\} = \{1, 2\}$ milliseconds, $E_j = 3$ W, $\forall j$ [13]. Other system parameters are shown as follows: $J = 3$, $K = 2$, $\tilde{\rho} = 1$, $\eta = 100$, $T = 60$, $W = 60$ MHz, $M = 100$, $\phi = 1.5$, $\xi = 54$, $\alpha_g = 0.05$, $\kappa = 5.12 \times 10^{-4}$, $\alpha = 10^{-5}$, $\beta = 2 \times 10^{-8}$, and $\varsigma = 2 \times 10^{-5}$ [11].

B. Performance evaluation

To evaluate the comparison algorithms, the following performance indicators are utilized i) RA success probability $P_s(t)$; ii) expected queue length per IoT device at minislot t , $E[Q_s(t)] =$

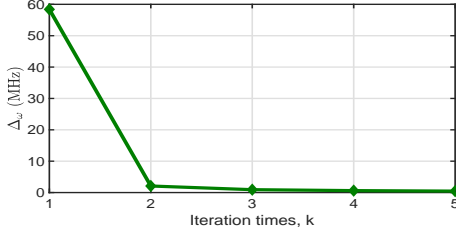
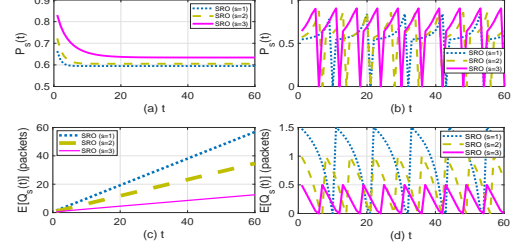


Fig. 3. The convergence curve of the SRO algorithm.

Fig. 4. Trends of $P_s(t)$ and $E[Q_s(t)]$.

$\mu_{a,s}(t)$; iii) total slice utility \bar{U} that is the objective function of (22).

We first evaluate the convergence mainly determined by that of the ADMM-based framework of the proposed SRO algorithm. We then leverage $\Delta_\omega = \sum_{s \in \mathcal{S}^I} |\omega_s^{(k+1)}(\bar{t}) - \omega_s^{(k)}(\bar{t})|$ to evaluate the convergence of the SRO algorithm. Fig. 3 illustrates the algorithm's convergence. It shows that SRO can converge after several iterations.

We next plot the tendency of the RA success probability $P_s(t)$ and the corresponding expected queue length $E[Q_s(t)]$ during a time slot in Fig. 4. Fig. 4(a) and 4(c) show the tendency of $P_s(t)$ and $E[Q_s(t)]$ in the case of $\{\gamma_s^{th}\} = \{1.8, 1.35, 0.9\}$ Kbits/minislot. Fig. 4(b) and 4(d) depict the tendency of $P_s(t)$ and $E[Q_s(t)]$ in the case $\{\gamma_s^{th}\} = \{5.8, 4.35, 2.9\}$ Kbits/minislot.

From Fig. 4, we obtain the following interesting conclusions: the queue of each IoT device is not stable when the queue serving rate γ_s^{th} is small. In this case, the average queue length monotonously increases over t . On the contrary, the queue of each IoT device is periodically flushed when a great queue serving rate is configured. The result that the maintained queue by each IoT device can be emptied verifies the correctness of the analysis of the RA process.

Let the IoT device intensity $\lambda^I = [900n, 900n, 900n]$ with $n \in \{6, 8, \dots, 26\}$. Under the existence of both mIoT and URLLC slices, we plot trends of the total slice utility \bar{U} and bursty URLLC slice utility \bar{U}^u w.r.t. n in Fig. 5 to understand the impact of the mIoT slices on the performance of all comparison algorithms. In this figure, $B = [b_{11}^u, \dots, b_{31}^u, b_{12}^u, \dots, b_{52}^u]$, $\omega^I = [\omega_{SRO}^I, \omega_{ACB_I}^I, \omega_{ACB_{II}}^I]$ MHz with ω_{SRO}^I , $\omega_{ACB_I}^I$ and $\omega_{ACB_{II}}^I$ representing the bandwidth allocated to mIoT slices by executing SRO, SRO-ACB_I, and SRO-ACB_{II} algorithms, respectively, and $\bar{U}^I = [\bar{U}_{SRO}^I, \bar{U}_{ACB_I}^I, \bar{U}_{ACB_{II}}^I]$ with \bar{U}_{SRO}^I denoting the achieved mIoT slice utility of SRO.

The following observations can be obtained from Fig. 5: i) when $n < 16$, all algorithms almost obtain the same \bar{U} , and the obtained utilities are robust to the average number of IoT

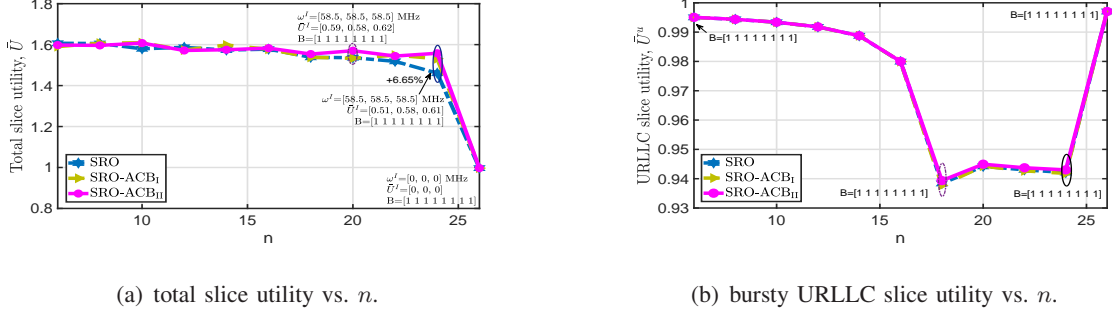
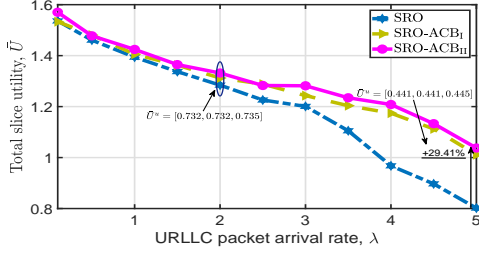
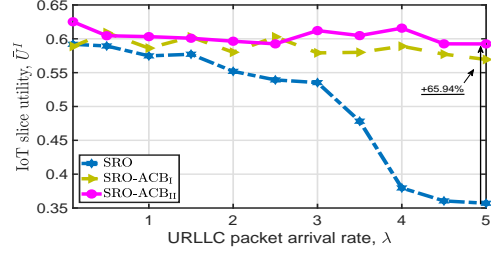
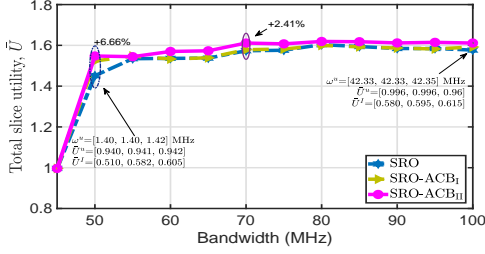
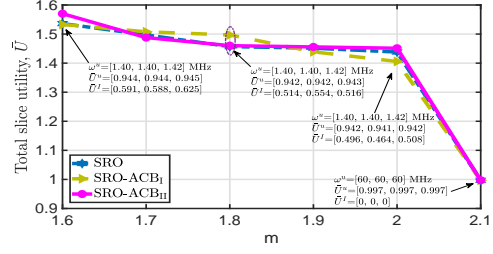


Fig. 5. Trends of the achieved total slice utilities and bursty URLLC slice utilities of all algorithms vs. n .

devices; ii) when $16 \leq n \leq 26$, the conclusion changes. For the SRO algorithm, its achieved \bar{U} decreases with an increasing n due to increasing interference. A great n , however, does not cause a significant decrease in the obtained \bar{U} by SRO-ACB_I and SRO-ACB_{II}. Thanks to the exploration of an access control scheme, both SRO-ACB_I and SRO-ACB_{II} can achieve greater \bar{U} than SRO. For example, compared with SRO, SRO-ACB_{II} improves \bar{U} by 6.65% when $n = 24$; iii) when $n = 26$, which means that the total average number of IoT devices reaches 70,200 devices, the RAN slicing system fails to create and manage mMTC slices as the QoS requirements of mMTC slices serving such a massive average number of devices cannot be simultaneously satisfied. In this case, all system resources are allocated to URLLC slices, and the maximum bursty URLLC slice utility is obtained; iv) as mMTC slices and URLLC slices share the system resources, an increasing n results in a decreasing \bar{U}^u ; Besides, it is interesting to find that the two access-control-based algorithms may not outperform SRO in terms of obtaining \bar{U}^u . It indicates that URLLC slices do not benefit from access control schemes of mMTC slices when changing n ; v) the RAN slicing system can always accommodate the QoS requirements of all URLLC devices.

Next, to understand the impact of URLLC slices on the performance of all comparison algorithms, we plot the trends of \bar{U} and the mMTC slice utilities obtained by all comparison algorithms w.r.t. URLLC packet arrival rate λ with $\lambda = \{0.1, 0.5, 1.0, \dots, 4.5, 5.0\}$ packets per unit time in Fig. 6. Similarly, the following notations are involved in Fig. 6: $\omega^u = [\omega_{SRO}^u, \omega_{ACB_I}^u, \omega_{ACB_{II}}^u]$, $\bar{U}^u = [\bar{U}_{SRO}^u, \bar{U}_{ACB_I}^u, \bar{U}_{ACB_{II}}^u]$ with ω_{SRO}^u and \bar{U}_{SRO}^u denoting the bandwidth allocated to URLLC slices and the URLLC slice utility obtained by running the SRO algorithm, respectively.

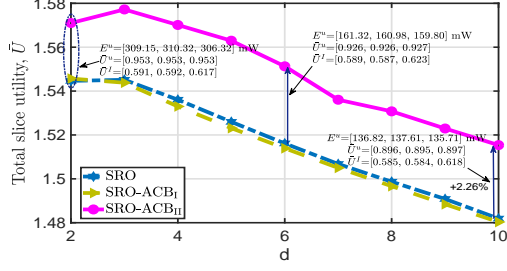
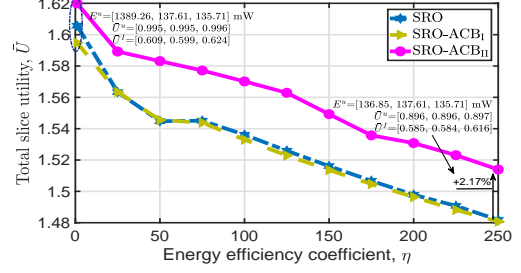
From Fig. 6, we can observe that: i) the obtained \bar{U} of all algorithms decrease with λ mainly due to the decrease of the bursty URLLC slice utility. Two algorithms adopting the access control scheme always achieve greater utilities \bar{U} than SRO. For example, when $\lambda = 5$, compared

(a) total slice utility vs. λ .(b) mIoT slice utility vs. λ .Fig. 6. Trends of the achieved total slice utilities and IoT slice utilities of all algorithms vs. λ .Fig. 7. Trend of achieved \bar{U} vs. system bandwidth.Fig. 8. Trend of achieved total slice utility vs. m .

with the SRO algorithm, the obtained \bar{U} of SRO-ACB_{II} is increased by 29.41%; ii) for all algorithms, the computed bandwidth for URLLC slices increases with an increasing λ . However, their obtained URLLC slice utilities \bar{U}^u are reduced owing to the increase of energy consumption; iii) SRO-ACB_{II} may achieve greater \bar{U} than SRO-ACB_I as a greater \bar{U}^I is obtained by reducing the number of interfering IoT devices; iv) the obtained mIoT slice utilities \bar{U}^I of SRO-ACB_I and SRO-ACB_{II} are robust to the URLLC packet arrival rate. The obtained \bar{U}^I of SRO decreases with an increasing λ ; v) an important observation is that the \bar{U}^I of the access-control-based SRO-ACB_I algorithm is 1.65 times that of the SRO algorithm when $\lambda = 5$. It explicitly reflects that mIoT slices can still benefit from access control schemes even though λ is changed.

Figs. 5 and 6 illustrate the situation of a given total system bandwidth. We next change the total bandwidth W and plot its impact on the obtained \bar{U} of all algorithms in Fig. 7.

The following conclusions can be obtained from Fig. 7: i) when $W = 45$ MHz, the QoS requirements of all IoT devices cannot be simultaneously satisfied. As a result, the total bandwidth is allocated to URLLC slices; ii) when W locates in the range of $(45, 55]$ MHz, the achieved total slice utilities \bar{U} of SRO and SRO-ACB_I increase with W . Owing to the utilization of the access control scheme, SRO-ACB_I and SRO-ACB_{II} obtain higher \bar{U} than SRO. For example,

Fig. 9. Trend of achieved total slice utility vs. d .Fig. 10. Trend of achieved total slice utility vs. η .

compared with the SRO algorithm, the SRO-ACB_{II} algorithm improves the achieved \bar{U} by 6.66% when $W = 50$ MHz; iii) when $W > 55$ MHz, all algorithms cannot remarkably improve \bar{U} .

At last, we discuss other crucial parameters' impact on the performance of the comparison algorithms. We reconfigure $\{\gamma_s^{th}\}$ of mIoT slices as $\gamma_1^{th} = 3.6m$, $\gamma_2^{th} = 2.7m$ and $\gamma_3^{th} = 1.8m$ Kbits/minislot with $m \in \{1.5, 1.6, \dots, 2.1\}$ and $\{D_s\}$ of URLLC slices as $D_1 = 0.00025d$ second and $D_2 = 0.0005d$ second with $d \in \{2, 3, \dots, 10\}$. The impact of QoS requirements of network slices on the total slice utility is plotted in Figs. 8 and 9. The impact of energy efficiency coefficient η is plotted in Fig. 10. In this figure, we denote the energy consumption of RRHs of all algorithms by $E^u = [E_{SRO}^u, E_{ACB_I}^u, E_{ACB_{II}}^u]$ with $E_{SRO}^u = \sum_{t=1}^T \sum_{s \in S^u} \sum_{i \in \mathcal{I}_s^u} b_{i,s}^u \text{tr}(\mathbf{G}_{i,s})$.

From these figures, the following observations can be achieved: i) the obtained utilities \bar{U} of all algorithms decrease with an increasing m . This is because a great m indicates that the accumulated IoT packets in the queue of each IoT device can be quickly emptied, and then a small $P_s(t)$ is obtained; ii) a great D_s will reduce RRHs' energy consumption. However, it also reduces the URLLC slice gain. Then, it may be hard to conclude the trend of \bar{U}^u w.r.t. D_s as the energy efficiency coefficient η significantly affects the value of \bar{U}^u ; iii) it is also uneasy to conclude the trend of \bar{U}^u w.r.t. η . An increasing η causes a decrease of RRHs' energy consumption. Yet, the value of \bar{U}^u is determined by the multiplier of η and E^u ; iv) the SRO-ACB_{II} algorithm may perform better than the SRO algorithm. However, the performance of the other access-control-based algorithm, SRO-ACB_I, is slightly worse than SRO. Besides, it cannot ensure that the \bar{U}^I obtained by the access-control-based algorithms are always higher than that of SRO. At sometimes, access control schemes may drag down the utility of the mIoT service.

To sum up, in the case of service multiplexing, RA control schemes for alleviating signal interference and enhancing mIoT slice utility may be preferred for mIoT slices. However,

considering both the CAPEX and the improvement of slice utility, RA control schemes should be carefully designed and employed because some RA control schemes may worsen the mIoT and total slice utilities.

IX. CONCLUSION

In this paper, we revisited the frame and minislot structure of a RAN slicing system to admit more IoT devices and proposed a queue evolution model to analyze the RACH of a randomly chosen IoT device. Based on the analysis result, we derived the closed-form expression of the RA success probabilities of the device with an unrestricted access control scheme and an ACB access control scheme. Next, we formulated the RAN slicing for mIoT and bursty URLLC service multiplexing as an optimization problem to optimally orchestrating RAN resources for mIoT slices and URLLC slices, and efficient mechanisms such as SAA and ADMM were exploited to mitigate the optimization problem. Simulation results showed that RA control schemes should be carefully designed and employed in the case of service multiplexing.

APPENDIX

A. Proof of Lemma 1

The work in [16] adopted a standard stochastic geometry method to derive the LT of the aggregated interference from interfering IoT devices. Different from [16], both the stochastic geometry method and a gamma-Poisson distribution are exploited to derive the result in this paper.

For the origin RRH, the LT of its aggregate interference from interfering IoT devices in s can be derived as

$$\begin{aligned}
 \mathcal{L}_{\mathcal{I}_s(t)}(\varpi_s) &= \mathbb{E}_{\mathcal{I}_s(t)} \left[e^{-\varpi_s \mathcal{I}_s(t)} \right] = \mathbb{E}_{\mathcal{I}_s(t)} \left[e^{-\varpi_s \sum_{m \in u_s^I \setminus \{o\}} \mathbb{1}(p_m \|d_m\|^{-\varphi} = \rho_o) \mathbb{1}(N_{a,s}(t) > 0) \mathbb{1}(f_m = f_o) \rho_o h_m} \right] \\
 &\stackrel{(a)}{=} \mathbb{E}_{u_s^I} \left[\prod_{m \in u_s^I \setminus \{o\}} \mathbb{E}_{h_m} \left[e^{-\varpi_s \mathbb{1}(P_m \|u_{m,s}\|^{-\varphi} = \rho_o) \mathbb{1}(N_{a,s}(t) > 0) \mathbb{1}(f_m = f_o) \rho_o h_m} \right] \right] \\
 &\stackrel{(b)}{=} \sum_{n=0}^{\infty} \mathbb{P}\{|Z_s| = n\} \prod_{m \in Z_s} \mathbb{E}_{h_m} \left[e^{-\varpi_s \rho_o h_m} \right] \stackrel{(c)}{=} \mathbb{P}\{|Z_s| = 0\} + \sum_{n=1}^{\infty} \mathbb{P}\{|Z_s| = n\} \left(\frac{1}{1 + \varpi_s \rho_o} \right)^n \\
 &\stackrel{(d)}{=} \tilde{\mathbb{P}}_{X_s}\{X_s = 1\} + \left\{ \sum_{n'=0}^{\infty} \tilde{\mathbb{P}}_{X_s}\{X_s = n'\} \left(\frac{1}{1 + \varpi_s \rho_o} \right)^{n'} - \sum_{n'=0}^1 \tilde{\mathbb{P}}_{X_s}\{X_s = n'\} \left(\frac{1}{1 + \varpi_s \rho_o} \right)^{n'} \right\} (1 + \varpi_s \rho_o)
 \end{aligned} \tag{39}$$

where $\varpi_s = \frac{\theta^{th}}{\rho_o}$, Z_s denotes the set of interfering IoT devices associated with the origin RRH in mIoT slice s , X_s represents the number of active IoT devices associated with the origin RRH

in s . According to the conclusion of Lemma 1 in [31], the probability mass function (PMF) $\tilde{\mathbb{P}}_{X_s}\{X_s = n'\}$ can be written as

$$\tilde{\mathbb{P}}_{X_s}\{X_s = n'\} = \frac{3.5^{3.5} \Gamma(n' + 3.5) \left(\frac{P_{nr,s}(t) P_{ne,s}(t) \lambda_s^I}{\lambda_R \xi F_s} \right)^{n'}}{\Gamma(3.5) (n')! \left(\frac{P_{nr,s}(t) P_{ne,s}(t) \lambda_s^I}{\lambda_R \xi F_s} + 3.5 \right)^{n' + 3.5}} \quad (40)$$

with $\Gamma(\cdot)$ being the gamma function. Besides, in (39), (a) follows from the i.i.d distribution of h_m and its further independence from the Poisson point process Φ_s or u_s^I ; (b) follows from the expectation of a discrete random variable; (c) follows from the LT over h_m ; (d) follows from the fact that the number of active IoT device in a specific Voronoi cell is one more than the number of active interfering IoT devices in this cell.

From (40), we can deduce that X_s ($s \in \mathcal{S}^I$) is a gamma-Poisson random variable with $X_s \sim \text{gamma-Poisson}(\alpha_s, 3.5)$ and $\alpha_s = \frac{P_{nr,s}(t) P_{ne,s}(t) \lambda_s^I}{3.5 \lambda_R \xi F_s}$. For a gamma-Poisson random variable $X_s \sim \text{gamma-Poisson}(\alpha, \beta)$, the following expression holds: $\mathbb{E}[e^{X_s}] = (1 + \alpha - \alpha e)^{-\beta}$. Thus, we can rewrite (39) as (8). This completes the proof.

B. Proof of Lemma 2

The work in [16] derived the expression of the intensity of accumulated packets μ_{Cum}^2 at the 2nd slot. However, they did not derive the expression of μ_{Cum}^t with $t \geq 3$, the detail derivation of which was different from that of the expression of μ_{Cum}^2 . Based on the results in [16], we derive the expression of the intensity of accumulated packets $\mu_{a,s}(t)$ and the expression of the non-empty probability $P_{ne,s}(t)$ for all $s \in \mathcal{S}^I$, $t > 1$.

As new endogenous packet arrivals in any IoT device at each minislot t is modelled as a Poisson distribution, the departure process of packets can be regarded as an approximated thinning process of new arrivals, where the thinning factor is related to the RA success probability. The number of accumulated packets in the queue of any IoT device can then be approximated as a Poisson distribution with intensity $\mu_{a,s}^t$ ($s \in \mathcal{S}^I$) after the thinning process in a specific minislot t ($t > 1$) [16].

Thus, we can derive the expression of $\mu_{a,s}^t$ ($t > 1$) via combining with the following facts

- **Fact 1:** the accumulated packets during the $t - 1$ -th minislot will contribute to the accumulated packets at the t -th minislot.
- **Fact 2:** the arrival packets during the $t - 1$ -th minislot will also contribute to the accumulated packets in the queue of an IoT device at the t -th minislot.

- **Fact 3:** an IoT device can send packets only if its preamble is successfully transmitted.
- **Fact 4:** at the same minislot, the new packet arrival process and the packet accumulated process are independent.

Similar as the Theorem 2 in [16], we can infer that at the 2nd minislot, for all $s \in \mathcal{S}^I$, $\mu_{a,s}^2$ depends on the intensity of new packet arrivals $\mu_{w,s}^1$ and the probability P_s^1 of a randomly selected IoT device at the 1st minislot, which is given by

$$\mu_{a,s}^2 = \mu_{w,s}^1 - x_s P_s^1 \left(1 - e^{-\mu_{w,s}^1}\right) \quad (41)$$

The detailed proof of (41) is omitted for brevity, and a similar proof can be found in Theorem 2 in [16].

Considering that $\mu_{a,s}(t)$ is non-negative at each minislot t , we have

$$\mu_{a,s}^2 = \left[\mu_{w,s}^1 - x_s P_s^1 \left(1 - e^{-\mu_{w,s}^1}\right) \right]^+ \quad (42)$$

Then, according to the definition of non-empty probability and the Poisson approximation, the non-empty probability of a randomly selected IoT device in mIoT slice $s \in \mathcal{S}^I$ at the 2nd minislot can be approximated as

$$P_{ne,s}^2 = 1 - \mathbb{P}\{N_{a,s}^2 = 0\} = 1 - e^{-\mu_{a,s}^2} \quad (43)$$

At the 3rd minislot, the intensity of accumulated data packets in the queue of a randomly selected IoT device can be derived as the following

$$\begin{aligned} \mu_{a,s}^3 &= P_s^2 \left(\sum_{n=1}^{\infty} \left([n - x_s]^+ \sum_{z=0}^n P_{N_{w,s}^2}(z) P_{N_{a,s}^2}(n - z) \right) \right) + (1 - P_s^2) \left(\sum_{n=1}^{\infty} n \sum_{z=0}^n P_{N_{w,s}^2}(z) P_{N_{a,s}^2}(n - z) \right) \\ &\stackrel{(a)}{=} P_s^2 \left[\sum_{n=1}^{\infty} \sum_{z=0}^n \frac{(\mu_{w,s}^2)^z e^{-\mu_{w,s}^2}}{z!} \frac{(\mu_{a,s}^2)^{n-z} e^{-\mu_{a,s}^2}}{(n-z)!} \times n - x_s \sum_{n=1}^{\infty} \sum_{z=0}^n \frac{(\mu_{w,s}^2)^z e^{-\mu_{w,s}^2}}{z!} \frac{(\mu_{a,s}^2)^{n-z} e^{-\mu_{a,s}^2}}{(n-z)!} \right]^+ + \\ &\quad (1 - P_s^2) \sum_{n=1}^{\infty} \sum_{z=0}^n \frac{(\mu_{w,s}^2)^z e^{-\mu_{w,s}^2}}{z!} \frac{(\mu_{a,s}^2)^{n-z} e^{-\mu_{a,s}^2}}{(n-z)!} \times n \\ &\stackrel{(b)}{=} \left[\mu_{w,s}^2 + \mu_{a,s}^2 - x_s P_s^2 \left(1 - e^{-\mu_{w,s}^2 - \mu_{a,s}^2}\right) \right]^+ \end{aligned} \quad (44)$$

where $P_{N_{w,s}^2}$ and $P_{N_{a,s}^2}$ represent the PMFs of new arrival packets and accumulated packets at the 2nd minislot, respectively. Besides, (a) follows from the fact: for any two independent Poisson distributions Φ_{X_1} and Φ_{X_2} , $\mathbb{P}_{X_1, X_2}(X_1 + X_2 = x) = \sum_{y=0}^x \mathbb{P}_{X_1}(X_1 = y) \mathbb{P}_{X_2}(X_2 = x - y)$; (b) holds as Φ_{X_1, X_2} is a two dimensional Poisson distribution with an intensity $\lambda_{X_1} + \lambda_{X_2}$, and $\sum_{x=1}^{\infty} \mathbb{P}_{X_1, X_2}(X_1 + X_2 = x) = 1 - \mathbb{P}_{X_1, X_2}(X_1 + X_2 = 0)$.

Similarly, we have

$$P_{ne,s}^3 = 1 - \mathbb{P}\{N_{a,s}^3 = 0\} = 1 - e^{-\mu_{a,s}^3} \quad (45)$$

When $t > 3$, since the accumulated packets evolution model of the queue of any IoT device is the similar as that at $t = 3$, we can extend the conclusion obtained at $t = 3$ to that at $t > 3$.

Therefore, we can obtain the closed-form expression of $\mu_{a,s}^t$ for all $s \in \mathcal{S}^I$ at $t > 1$ with

$$\mu_{a,s}^t = \left[\mu_{w,s}^{t-1} + \mu_{a,s}^{t-1} - x_s P_s^{t-1} \left(1 - e^{-\mu_{w,s}^{t-1} - \mu_{a,s}^{t-1}} \right) \right]^+ \quad (46)$$

and

$$P_{ne,s}^t = 1 - \mathbb{P}\{N_{a,s}^t = 0\} = 1 - e^{-\mu_{a,s}^t} \quad (47)$$

This completes the proof.

C. Proof of Lemma 4

The 2nd degree Taylor expansion of $\tilde{P}_m^{(k)}$ at the local point $\omega_m^{(k,q)}$ is

$$\tilde{P}_{2,m}^{(k)} = \sum_{j=0}^2 \frac{1}{j!} \left[\sum_{s \in \mathcal{S}^I} (\omega_{sm} - \omega_{sm}^{(k,q)}) \frac{\partial}{\partial \omega_{sm}^{(k,q)}} \right]^j \tilde{P}_m^{(k)}|_{\omega_m^{(k,q)}} \quad (48)$$

The 3rd degree Taylor expansion of $\tilde{P}_m^{(k)}$ at $\omega_m^{(k,q)}$ must be more accurate than $\tilde{P}_{2,m}^{(k)}$ with

$$\tilde{P}_{3,m}^{(k)} = \tilde{P}_{2,m}^{(k)} + \frac{1}{3!} \left[\sum_{s \in \mathcal{S}^I} (\omega_{sm} - \omega_{sm}^{(k,q)}) \frac{\partial}{\partial \omega_{sm}^{(k,q)}} \right]^3 \tilde{P}_m^{(k)}|_{\omega_m^{(k,q)}} \quad (49)$$

Since the error of $\tilde{P}_{2,m}^{(k)}$ is not greater than the maximum difference between $\tilde{P}_{3,m}^{(k)}$ and $\tilde{P}_{2,m}^{(k)}$, we have

$$R_2(\omega_m) = \max \left\{ \frac{1}{3!} \left[\sum_{s \in \mathcal{S}^I} (\omega_{sm} - \omega_{sm}^{(k,q)}) \frac{\partial}{\partial \omega_{sm}^{(k,q)}} \right]^3 \tilde{P}_m^{(k)}|_{\omega_m^{(k,q)}} \right\} \quad (50)$$

In (50), $\omega_m^{(k,q)}$ is a constant vector, the max operation will not affect the constant vector and the vector ω_m . For any $s \in \mathcal{S}^I$, the maximum value obtainable by $\frac{\partial^3 \tilde{P}_m^{(k)}|_{\omega_m^{(k,q)}}}{\partial \omega_{sm}^{3(k,q)}}$ will not exceed the greatest value of that derivative in the interval $[\hat{\omega}_{sm}^{lb}, S_{sm}^*]$. Additionally, the maximum value of $\frac{\partial^3 \tilde{P}_m^{(k)}|_{\omega_m^{(k,q)}}}{\partial \omega_{sm}^{3(k,q)}}$ will generally occur at one of the endpoints of the interval $[\hat{\omega}_{sm}^{lb}, S_{sm}^*]$. Therefore, we obtain (35). This completes the proof.

D. Proof of Lemma 5

For all $i \in \mathcal{I}^u$, $s \in \mathcal{S}^I$, $m \in \mathcal{M}$, a feasible way of proving that $\text{rank}(\mathbf{G}_{i,sm}) \leq 1$ is to utilize the Lagrange method. However, owing to the complicated expression of $W^u(\mathbf{r}_m)$ w.r.t. $\mathbf{G}_{i,sm}$ it will be uneasy to do that. Fortunately, we find that the proof can be conducted if a family of auxiliary variables is introduced.

For the constraint (24d), if we introduce the auxiliary variables $\{\nu_{i,sm}\}$ and let

$$\frac{\text{tr}(\mathbf{H}_{i,sm}\mathbf{G}_{i,sm})}{\phi\sigma_{i,s}^2} \geq \nu_{i,sm}, \forall i \in \mathcal{I}_s^u, s \in \mathcal{S}^u, m \in \mathcal{M} \quad (51)$$

then (24d) is equivalent to

$$\sum_{s \in \mathcal{S}^I} (1 + \alpha_g) \omega_{sm}(\bar{t}) + W^u(\mathbf{f}_m) \leq W, \text{ and } (51) \quad (52)$$

where $\mathbf{f}_m = \{f_{i,sm}; i \in \mathcal{I}_s^u, s \in \mathcal{S}^u\}$ and

$$f_{i,sm} = \frac{L_{i,s}^u}{\log_2(1 + \nu_{i,sm})} + \frac{(Q^{-1}(\beta))^2}{2 \log_2^2(1 + \nu_{i,sm})} + \frac{(Q^{-1}(\beta))^2}{2 \log_2^2(1 + \nu_{i,sm})} \sqrt{1 + \frac{4L_{i,s}^u \log_2(1 + \nu_{i,sm})}{(Q^{-1}(\beta))^2}} \quad (53)$$

We omit the proof of the equivalence as a similar proof can be found in the proof section of constraints' equivalence in [11].

The partial Lagrangian function of (37) can be written as

$$L(\dots) = \sum_{s \in \mathcal{S}^u} \sum_{i \in \mathcal{I}_s^u} \left[\frac{\tilde{\rho}\eta}{M} \text{tr}(\mathbf{G}_{i,sm}) + \sum_{j \in \mathcal{J}} \bar{\lambda}_{jm} \text{tr}(b_{i,sm}^{u(k,q)} \mathbf{Z}_j \mathbf{G}_{i,sm}) - \bar{\mu}_{i,sm} \frac{\text{tr}(\mathbf{H}_{i,sm}\mathbf{G}_{i,sm})}{\phi\sigma_{i,s}^2} - \bar{\mathbf{X}}_{i,sm} \odot \mathbf{G}_{i,sm} \right] \quad (54)$$

where $\bar{\lambda}_{jm}$, $\bar{\mu}_{i,sm}$, and $\bar{\mathbf{X}}_{i,sm}$ are Lagrangian multipliers corresponding to constraints (24c), (51) and (24e), \odot is the matrix dot product operator. Besides, only terms related to $\mathbf{G}_{i,sm}$ are included in this function for brevity.

According to the Karush-Kuhn-Tucker (KKT) conditions, the necessary condition for obtaining the optimal matrix power at the (k, q) -th iteration $\mathbf{G}_{i,sm}^{(k,q)\star}$ is given by

$$\frac{\partial L(\dots)}{\partial \mathbf{G}_{i,sm}^{(k,q)\star}} = \frac{\tilde{\rho}\eta}{M} \mathbf{I}_{i,sm} + \sum_{j \in \mathcal{J}} \bar{\lambda}_{jm} b_{i,sm}^{u(k,q)} \mathbf{Z}_j - \frac{\bar{\mu}_{i,sm} \mathbf{H}_{i,sm}}{\phi\sigma_{i,s}^2} - \mathbf{X}_{i,sm} = 0 \quad (55)$$

where $\mathbf{I}_{i,sm} \in \mathbb{R}^{JK \times JK}$ is an identity matrix.

Then, we can conclude that $\text{rank}(\mathbf{X}_{i,sm}) \geq JK - 1$. The reasons are i) $\bar{\lambda}_{jm}$, $b_{i,sm}^{u(k,q)}$, and $\bar{\mu}_{i,sm}$ are nonnegative and the matrix $\mathbf{I}_{i,sm}$ is full rank; ii) $\text{rank}(\mathbf{H}_{i,sm}) \leq 1$.

Next, according to the complementary slackness condition, we have

$$\mathbf{X}_{i,sm} \mathbf{G}_{i,sm}^{(k,q)\star} = 0 \quad (56)$$

Based on (56) and the rank result of $\mathbf{X}_{i,sm}$, we can conclude that $\text{rank}(\mathbf{G}_{i,sm}^{(k,q)\star}) \leq 1$. This completes the proof.

REFERENCES

- [1] Ericsson, “Cellular networks for massive IoT,” Ericsson, Stockholm, Sweden, Tech. Rep. Uen 284 23-3278, Jan. 2016.
- [2] Nokia, “LTE evolution for IoT connectivity,” Nokia, Espoo, Finland, Tech. Rep. SR1702006775EN.
- [3] S. Xing, X. Wen, Z. Lu, Q. Pan, and W. Jing, “A novel distributed queuing-based random access protocol for narrowband-IoT,” in *ICC 2019-2019 IEEE International Conference on Communications (ICC)*. IEEE, 2019, pp. 1–7.
- [4] H. S. Jang, H.-S. Park, and D. K. Sung, “A non-orthogonal resource allocation scheme in spatial group based random access for cellular M2M communications,” *IEEE Trans. Veh. Technol.*, vol. 66, no. 5, pp. 4496–4500, 2016.
- [5] Z. Zhang, Y. Li, C. Huang, Q. Guo, C. Yuen, and Y. L. Guan, “DNN-aided block sparse bayesian learning for user activity detection and channel estimation in grant-free non-orthogonal random access,” *IEEE Trans. Veh. Technol.*, vol. 68, no. 12, pp. 12 000–12 012, 2019.
- [6] N. Alliance, “5G white paper,” *Next generation mobile networks, white paper*, vol. 1, 2015.
- [7] P. Rost, C. Mannweiler, D. S. Michalopoulos, C. Sartori, V. Sciancalepore, N. Sastry, O. Holland, S. Tayade, B. Han, D. Bega *et al.*, “Network slicing to enable scalability and flexibility in 5G mobile networks,” *IEEE Commun. Mag.*, vol. 55, no. 5, pp. 72–79, 2017.
- [8] P. Popovski, K. F. Trillingsgaard, O. Simeone, and G. Durisi, “5G wireless network slicing for eMBB, URLLC, and mMTC: A communication-theoretic view,” *IEEE ACCESS*, vol. 6, pp. 55 765–55 779, 2018.
- [9] I. Budhiraja, S. Tyagi, S. Tanwar, N. Kumar, and J. J. Rodrigues, “Tactile internet for smart communities in 5G: An insight for NOMA-based solutions,” *IEEE Trans. Ind. Inform.*, vol. 15, no. 5, pp. 3104–3112, 2019.
- [10] A. Ksentini and N. Nikaiein, “Toward enforcing network slicing on RAN: Flexibility and resources abstraction,” *IEEE Commun. Mag.*, vol. 55, no. 6, pp. 102–108, 2017.
- [11] P. Yang, X. Xi, Q. S. T. Quek, J. Chen, X. Cao, and D. Wu, “How should I orchestrate resources of my slices for bursty URLLC service provision?” Tech. Rep. arXiv 1912.00579, Dec. 2019, <https://arxiv.org/pdf/1912.00579.pdf>.
- [12] 3GPP, “Cellular system support for ultra low complexity and low throughput Internet of Things,” the third-generation partnership project, Tech. Rep. 45.820, Nov. 2015.
- [13] J. Tang, B. Shim, and T. Q. Quek, “Service multiplexing and revenue maximization in sliced C-RAN incorporated with URLLC and multicast eMBB,” *IEEE J. SEL. AREAS COMMUN.*, vol. 37, no. 4, pp. 881–895, 2019.
- [14] H. Zhang, C. Jiang, N. C. Beaulieu, X. Chu, X. Wang, and T. Q. Quek, “Resource allocation for cognitive small cell networks: A cooperative bargaining game theoretic approach,” *IEEE Trans. Wirel. Commun.*, vol. 14, no. 6, pp. 3481–3493, 2015.
- [15] M. N. Soorki, W. Saad, M. H. Manshaei, and H. Saidi, “Stochastic coalitional games for cooperative random access in M2M communications,” *IEEE Trans. Wirel. Commun.*, vol. 16, no. 9, pp. 6179–6192, 2017.
- [16] N. Jiang, Y. Deng, X. Kang, and A. Nallanathan, “Random access analysis for massive IoT networks under a new spatio-temporal model: A stochastic geometry approach,” *IEEE TC*, vol. 66, no. 11, pp. 5788–5803, 2018.
- [17] M. Grau, C. H. Foh, A. ul Quddus, and R. Tafazolli, “Preamble barring: A novel random access scheme for machine type communications with unpredictable traffic bursts,” in *2019 IEEE 90th Vehicular Technology Conference (VTC2019-Fall)*. IEEE, 2019, pp. 1–7.
- [18] 3GPP, “Study on RAN improvements for machine-type communications,” 3GPP, Sophia, Antipolis, France, Tech. Rep. TR 37.868 V11.0.0, Sep. 2011.

- [19] M. Haenggi, *Stochastic geometry for wireless networks*. Cambridge University Press, 2012.
- [20] H. ElSawy and E. Hossain, "On stochastic geometry modeling of cellular uplink transmission with truncated channel inversion power control," *IEEE Trans. Wirel. Commun.*, vol. 13, no. 8, pp. 4454–4469, 2014.
- [21] M. Becchi, "From poisson processes to self-similarity: a survey of network traffic models," *Washington University in St. Louis*, no. CSE 567.06.
- [22] A. Anand and G. de Veciana, "Resource allocation and HARQ optimization for URLLC traffic in 5G wireless networks," *IEEE J. SEL. AREAS COMMUN.*, vol. 36, no. 11, pp. 2411–2421, 2018.
- [23] Z. Hou, C. She, Y. Li, T. Q. Quek, and B. Vucetic, "Burstiness-aware bandwidth reservation for ultra-reliable and low-latency communications in tactile internet," *IEEE J. SEL. AREAS COMMUN.*, vol. 36, no. 11, pp. 2401–2410, 2018.
- [24] W. Yang, G. Durisi, T. Koch, and Y. Polyanskiy, "Quasi-static multiple-antenna fading channels at finite blocklength," *IEEE Trans. Inf. Theory*, vol. 60, no. 7, pp. 4232–4265, 2014.
- [25] J. Tang, T. Q. Quek, T.-H. Chang, and B. Shim, "Systematic resource allocation in cloud RAN with caching as a service under two timescales," *IEEE Trans. Commun.*, vol. 67, no. 11, pp. 7755–7770, 2019.
- [26] S. Kim, R. Pasupathy, and S. G. Henderson, "A guide to sample average approximation," in *Handbook of simulation optimization*. Springer, 2015, pp. 207–243.
- [27] S. Boyd, N. Parikh, E. Chu, B. Peleato, J. Eckstein *et al.*, "Distributed optimization and statistical learning via the alternating direction method of multipliers," *Foundations and Trends® in Machine learning*, vol. 3, no. 1, pp. 1–122, 2011.
- [28] E. Karipidis, N. D. Sidiropoulos, and Z.-Q. Luo, "Quality of service and max-min fair transmit beamforming to multiple cochannel multicast groups," *IEEE Trans. Signal Process.*, vol. 56, no. 3, pp. 1268–1279, 2008.
- [29] W.-K. K. Ma, "Semidefinite relaxation of quadratic optimization problems and applications," *IEEE Signal Process. Mag.*, vol. 1053, no. 5888/10, 2010.
- [30] P. Yang, X. Cao, X. Xi, Z. Xiao, and D. Wu, "Three-dimensional drone-cell deployment for congestion mitigation in cellular networks," *IEEE Trans. Veh. Technol.*, vol. 67, no. 10, pp. 9867–9881, 2018.
- [31] S. M. Yu and S.-L. Kim, "Downlink capacity and base station density in cellular networks," in *2013 11th international symposium and workshops on modeling and optimization in mobile, ad hoc and wireless networks (WiOpt)*. IEEE, 2013, pp. 119–124.